



Controls on Reactive Oxygen Species Cycles in Yellowstone Hot Springs: Implications for Biosignature Preservation on Mars

Nancy W. Hinman^{1*}, Megan A. Mave¹, Leanne C. Powers², Philippe Schmitt-Kopplin^{3,4}, Nathalie A. Cabrol⁵ and Michael Gonsior²

¹University of Montana, Geosciences Department, Missoula, MT, United States, ²University of Maryland Center for Environmental Science, Chesapeake Biological Laboratory, Cambridge, MD, United States, ³Helmholtz Zentrum Muenchen - German Research Center for Environmental Health, Research Unit Analytical BioGeoChemistry, Neuherberg, Germany, ⁴Technische Universität München, Chair of Analytical Food Chemistry, Weihenstephan, Germany, ⁵Carl Sagan Center, The SETI Institute, Mountain View, CA, United States

OPEN ACCESS

Edited by:

Chandra Sivaram,
Indian Institute of Astrophysics, India

Reviewed by:

Josep M. Trigo-Rodríguez,
Institute of Space Sciences, Spanish
National Research Council (CSIC),
Spain

Priya Hasan,
Maulana Azad National Urdu
University, India

*Correspondence:

Nancy W. Hinman
nancy.hinman@umontana.edu

Specialty section:

This article was submitted to
Astrobiology,
a section of the journal
Frontiers in Astronomy and Space
Sciences

Received: 17 June 2021

Accepted: 05 May 2022

Published: 01 July 2022

Citation:

Hinman NW, Mave MA, Powers LC,
Schmitt-Kopplin P, Cabrol NA and
Gonsior M (2022) Controls on Reactive
Oxygen Species Cycles in Yellowstone
Hot Springs: Implications for
Biosignature Preservation on Mars.
Front. Astron. Space Sci. 9:727015.
doi: 10.3389/fspas.2022.727015

Early Earth and Mars had analogous environments. While life developed on our planet, the question of whether it did on Mars remains to be answered. Hot spring deposits are compelling targets for exploration because of their high habitability and potential to retain morphological and chemical biosignatures. As a result in this study, we aim to better understand the potential for biosignature preservation in Fe-bearing hydrothermal systems. Understanding oxidation-reduction reactions involving Fe in hot springs is a key step in elucidating the preservation process. Fe reacts readily with reactive oxygen species (ROS), which are produced in hot spring surface waters through photochemical processes. Furthermore, Fe³⁺ can bind to cell membranes and preserve complex organic molecules (i.e., biomarkers). ROS formation is typically controlled by photoreactions with dissolved organic matter (DOM). However, Fe redox reactions more likely control ROS formation in these Fe-bearing systems. We deconvolved the relationship of ROS with Fe in hot springs and evaluated the role that DOM and dissolved organic sulfur (DOS) may have in ROS production. To better understand these coupled systems, field and laboratory experiments were conducted in hot springs of Yellowstone National Park. *In situ* H₂O₂ concentrations observed in these hot springs were comparable to, or higher than, those of other high-temperature systems. Reaction rates determined by measuring concentrations after specified time intervals varied based on water compositions and the presence of particulate or dissolved matter. Fe speciation (photochemical reactivity), concentration, and solubility further determined ROS cycling rates. Specifically, photochemically active Fe enhanced both ROS formation and decay rates depending on incident UV irradiance, and rates increased along with Fe concentration and solubility (i.e., in acidic conditions). Better understanding how ROS and Fe cycle in predominantly abiotic conditions will eventually aid in distinguishing between biosignatures and abiotic substances in the rock record.

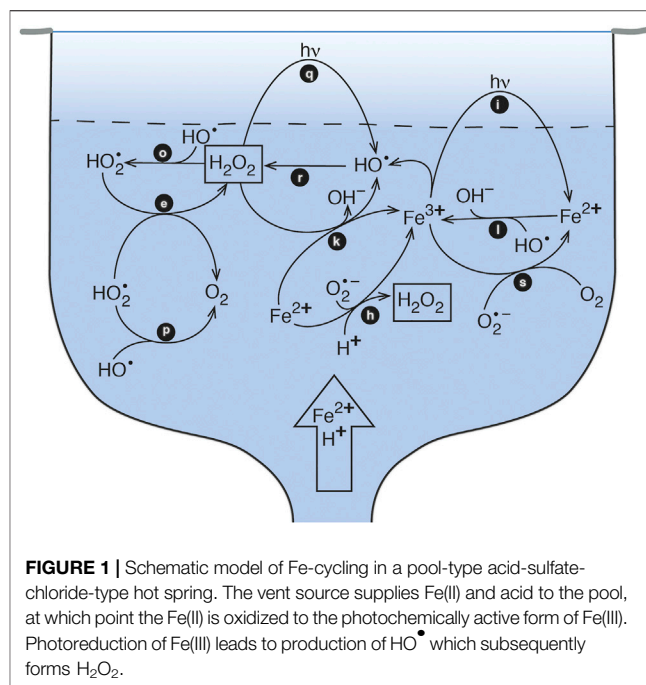
Keywords: reactive oxygen species, photochemistry, hot spring, ultrahigh resolution mass spectrometry (FT-ICR MS), organic sulfur, mars, biosignature

1 INTRODUCTION

Biosignatures can be preserved via rapid entombment by minerals precipitated from solution (Farmer and Des Marais, 1999; Des Marais and Walter, 2019). Consequently, aqueous environments with oversaturated minerals have a high potential for preserving biosignatures. Indeed, hydrothermal systems exhibit high preservation potentials as they contain ample dissolved minerals that become oversaturated as physicochemical conditions change (e.g., Des Marais and Walter, 2019 and references therein). Fe-rich systems have questionable ability to preserve organic biosignatures (Tan and Sephton, 2020), and so there are fewer reports of entombment in hydrothermal systems by iron minerals relative to reports about silica (e.g., Konhauser and Ferris, 1996; Jones and Renaut, 2007; Parenteau et al., 2014; Parenteau and Cady, 2010; Fernández-Remolar et al., 2008; Pierson and Parenteau, 2000; silica: Cady and Farmer, 1996; Alleon et al., 2016; Cady et al., 2003; Farmer and Des Marais, 1999; Campbell et al., 2015; Kyle et al., 2007; Jones et al., 2001). Fe(III) can, in turn, oxidize (and thus destroy) organic matter (e.g., Klein, 2005; Huang et al., 2020; Tan and Sephton, 2020). Yet, recent studies have shown that under the right chemical conditions, Fe may actually enhance biosignature preservation compared to Si alone (Parenteau and Cady, 2010; Parenteau et al., 2014 and references therein). Parenteau and Cady (2010) showed that ferrihydrite can adhere to negatively charged cell surfaces, which may protect cell membranes from decay. Then Fe-oxyhydroxides are isolated from their environment by the co-precipitation of silica (Konhauser and Ferris, 1996; Parenteau and Cady, 2010), and lipid biomarkers survive the earliest stages of taphonomic preservation (Parenteau et al., 2014). If this process occurs rapidly, organic molecules can become preserved within a Fe-oxide and Si-oxide crust. Thus the speciation of dissolved iron and solubility of iron oxyhydroxide phases could have a role in preservation of biosignatures in silica-rich hot springs, and consequently factors affecting the rates and sequences of dissolved iron transitions become important in understanding the preservation processes.

Volcanic hydrothermal systems were most likely widespread on Mars from 4.1 to 3.7 Ga (Baratoux et al., 2011; Ruff et al., 2011; Ruff and Farmer, 2016). These hydrothermal systems were likely acidic and Fe-rich because Fe is the most abundant crustal element on Mars after Si and O (Cockell, 2000). Meteorites also would have supplied catalytic minerals to the surfaces of both young planets (e.g., Cohen et al., 2000; Rotelli et al., 2016; Bottke et al., 2012; Saladino et al., 2013). Consequently, surface water could have been subjected to strong meteoritic flux while hydrothermal waters related to volcanic activity would also be influenced by the chemistry of volcanic rocks.

Early Mars was potentially hospitable with a comparable UV flux comparable to that of early Earth, (Cockell, 2000). So, life could have developed on early Mars around the same time it did on Earth (e.g., Cabrol, 2018; McMahon et al., 2018). Subaerial hot springs have recently been proposed as one possible location for the emergence of life on Earth (Damer and Deamer, 2015; van Kranendonk, 2018; van Kranendonk et al., 2021). Therefore, if life



developed on Mars, it was most likely in these metal-rich hydrothermal systems. But are terrestrial hot springs, many of which are oxygenated, appropriate analogs for a largely anaerobic early Mars? The answer to this question is yes. Although many hot springs are at least partially oxygenated, they are relevant to the anoxic conditions of early Earth and Mars because reactive oxygen species could form during UV irradiation of water in the atmosphere and on the surface irrespective of the presence of oxygen (e.g., Wang and Liu, 2014). So, from an astrobiological standpoint, terrestrial hot springs are important analogs because they are habitable and have high preservation potential despite the differences in oxygen content between current Earth conditions and early Earth and Mars. Consequently, a better understanding of abiotic processes that affect redox conditions in these environments is key. Yet, some potentially major controls on redox chemistry in hot springs are largely unstudied. Reactive oxygen species are one such control.

Controls on ROS formation include mixing, depth, and clarity of the water column, temperature, pH, organic matter, and water composition. Herein, we focus on formation and decay mechanisms associated with Fe cycling in hot springs. Field studies were designed to characterize H₂O₂ cycling in an acidic, Fe-bearing hot spring and in a low-metal, alkaline chloride hot spring. Laboratory studies were conducted as well to isolate H₂O₂ formation and decay pathways in a controlled environment. These experiments were designed to determine the effects of 1) water type, 2) Fe concentrations and speciation, and 3) particulate and soluble matter on H₂O₂ formation and decay. Herein we present a model for Fe-induced, H₂O₂ cycling in Fe-bearing hot springs and estimate contributions from reactions involving particulate matter, superoxide, and dissolved Fe species (**Figure 1**). By improving our understanding of chemical cycles in these

TABLE 1 | Reaction equations and rate constants for reactions in text and **Figure 1**.

	Equation	Reaction Rate (M ⁻¹ s ⁻¹)	Source
A	CDOM + <i>hν</i> → CDOM*		
B	CDOM* + O ₂ → CDOM ⁺ + O ₂ ^{•-}		
C	O ₂ ^{•-} + H ⁺ → HO ₂ [•]	pK _a = 4.8	Bielski et al. (1985)
D	HO ₂ [•] + O ₂ ^{•-} + H ⁺ → H ₂ O ₂ + O ₂	9.7 × 10 ⁷	Bielski et al. (1985)
E	HO ₂ [•] + HO ₂ [•] → O ₂ + H ₂ O ₂	8.3 × 10 ⁵	Bielski et al. (1985)
F	Fe(III)-DOM(aq) + <i>hν</i> → Fe(II) + DOM* ⁺		e.g., Faust and Allen (1993)
G	Fe(II) + O ₂ → Fe(III) + O ₂ ^{•-}	5.5 × 10 ⁻⁵	Wang and Liu (2014)
H	Fe ²⁺ + H ⁺ + O ₂ ^{•-} → Fe ³⁺ + H ₂ O ₂	1.0 × 10 ⁷	Rush and Bielski (1985)
I	Fe(OH) ²⁺ + <i>hν</i> → Fe ²⁺ + OH ⁻	2.04 × 10 ⁻³ (est)	Wang and Liu (2014)
J	DOM + HO [•] → LMWC + CO ₂ + H ₂ O		Huang et al. (2020)
K	Fe ²⁺ + H ₂ O ₂ → OH ⁻ + Fe ³⁺ + HO [•]	52.4, 76	Kremer. (2003), Walling (1975)
L	Fe ²⁺ + HO [•] → Fe ³⁺ + OH ⁻	-	Wang et al. (2016)
M	O ₂ ^{•-} + H ₂ O ₂ \xrightarrow{Fe} O ₂ + HO [•] + HO ⁻		Koppenol, 2001; Liovich and Fridovich, 2002
N	Fe(III)-DOM(aq) + <i>hν</i> → Fe(II) + DOM* ⁺		Zuo and Hoigne, (1992)
O	H ₂ O ₂ + HO [•] → HO ₂ [•]	4.51 × 10 ⁻³	Benkelberg and Warneck (1995)
P	HO ₂ [•] + HO [•] → O ₂ + H ₂ O	3.1 × 10 ⁹	Ross and Ross (1977)
Q	H ₂ O ₂ + <i>hν</i> → HO [•]	-	Vaghjiani et al. (1992)
R	2HO [•] → H ₂ O ₂	5.2 × 10 ⁹	Farhatziz and Ross (1977)
S	Fe ³⁺ + O ₂ ^{•-} → Fe ²⁺ + O ₂	1.5 × 10 ⁸	Rush and Bielski (1985)
T	M ⁽ⁿ⁾⁺ + H ₂ O ₂ → 2M ⁽ⁿ⁺¹⁾⁺ + 2HO ⁻		Generic Fenton reaction
U	2M ⁽ⁿ⁺¹⁾⁺ + H ₂ O ₂ → 2M ⁽ⁿ⁾⁺ + O ₂ + 2H ⁺		Generic Haber Weiss reaction, alternative notation

systems, we will be able to refine where and how we search for evidence of early life on Earth and Mars.

Reactive oxygen species (ROS) are ubiquitous in the hydrosphere, biosphere, and atmosphere on Earth. They shape the speciation and oxidation state of biologically important elements (e.g., Fe, Cu, As, Mn, S). Thereby, ROS also influence microbial ecology and metabolic strategies (Moffett and Zika, 1987; McKnight et al., 1988; Wilson et al., 2000a; Parenteau et al., 2014; Mesle et al., 2017). Hydrogen peroxide (H₂O₂) can serve as a proxy for other ROS, such as the hydroxyl (HO[•]), hydroperoxyl (HO₂[•]), singlet oxygen (¹O₂), and superoxide (O₂^{•-}) radicals. H₂O₂ is rapidly produced when other ROS are abundant and degraded when they are limited. Its relatively long half-life - a few hours for lakes and coastal waters (Cooper and Lean, 1989; O'Sullivan et al., 2005 to days for open ocean waters (Avery et al., 2005; Yuan et al., 2017) - makes H₂O₂ easier to measure compared to other ROS. Consequently, H₂O₂ has been measured in marine, fluvial, lacustrine, and geothermal surface water, groundwater, and atmospheric water (Holm et al., 1987; Scully et al., 1996; Wilson et al., 2000a; Cooper et al., 2000; Scott et al., 2003; He et al., 2010; Mesle et al., 2017).

On Earth, the majority of H₂O₂ is formed by photochemical reactions in surface waters (e.g., Cooper et al., 1994, 2000; Scully et al., 1996). H₂O₂ production occurs via the excitation of chromophoric dissolved organic carbon (CDOM) by UV radiation (280–400 nm) (Eqs. 1–4, Table 1; see Sharpless and Blough, 2014; Cooper et al., 1994; Huang et al., 2020; Blough and Zepp, 1995; Bielski et al., 1985); although this charge-transfer mechanism in DOM remains confounding (Blough and Del Vecchio, 2018; McKay et al., 2018).



CDOM absorbs light, e⁻ is transferred from ground state to form an excited state (CDOM*), and most likely through intramolecular charge transfer, create one-electron reductants (CDOM^{*-/•+}) (Zhang et al., 2012).



e⁻ is transferred to molecular oxygen, forming O₂[•]



Pronation (pK = 4.8; Zhang et al., 2012).



Dismutation of HO₂[•] forms H₂O₂, O₂, and OH[•]

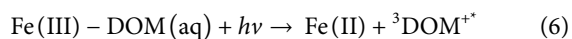


Dismutation of HO₂[•] forms H₂O₂ and O₂

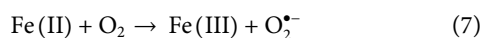
However, O₂^{•-} decay in natural waters can proceed via other routes including reactions with metals (e.g., iron, manganese, and copper) or DOM (Heller and Croot 2010a,b; Wuttig et al., 2013; Voelker et al., 2000). Petasne and Zika, 1997) found that a large fraction (24–41%) of O₂^{•-} photoproduction does not lead to its H₂O₂ based on irradiations of coastal seawater with and without additions of the enzyme superoxide dismutase (SOD), which forces a 2:1 stoichiometry between O₂^{•-} and H₂O₂ with a rate constant of >10⁹ M⁻¹ s⁻¹. Subsequent work found that additions of SOD increased the concentrations of photoproduced H₂O₂ during irradiations of Suwannee River Fulvic Acid (SRFA) solutions (Garg et al., 2011). Using the same approach, Powers and Miller (2016) found increasing O₂^{•-}:H₂O₂ ratios from 1.9 to 3.4 from riverine to offshore waters and closer to 4:1 in seawater. Furthermore, assuming that the photoproduction of one-electron reducing intermediates provides estimates for initial O₂^{•-} photoproduction rates, Zhang and Blough (2016) found that

$O_2^{\bullet-}$ formation was 6–13 times higher than H_2O_2 formation, well above the 2:1 stoichiometry estimated from $O_2^{\bullet-}$ dismutation. Thus, for oxygenated surface waters, these results suggest that superoxide dismutation (Eqs. 1, 2) is not the dominant pathway for superoxide decay, but rather oxidative sinks (possibly in the DOM pool) that do not return superoxide to molecular oxygen and therefore do not lead to H_2O_2 formation.

Metal redox reactions (Table 1, Eqs. 6–8) are considered less important sources of H_2O_2 in surface waters (Moffett and Zafriou, 1990; Cooper et al., 2000). While this may hold true in waters with high DOM and low metal concentrations, it is likely that metal redox cycling is a significant source of H_2O_2 when metals are present (Eqs. 6–9; e.g., Johnson et al., 1994; Paris et al., 2011; Wang and Liu, 2014; Chen and Browne, 2018). Prior work shows that H_2O_2 production rates in hot springs environments vary with pH and transition metal concentrations (Fe, Mn, and Cu) (Wilson et al., 2000a; Mesle et al., 2017), which is consistent with reports of H_2O_2 production rates in experimental and other natural systems (Mopper and Zhou, 1990; Zafriou et al., 1998). Environmental conditions, i.e., pH, concentrations of inorganic ions, and DOM, affect the reaction mechanism because such conditions control metal speciation. For example, Fe(III) hydrolysis speciation is a function of pH and consequently, the actual mechanism of direct photoreduction of iron involves either an organic Fe(III) complex (Eqs. 6, 9) or a hydrolysis product and not the free ion. Note that the latter photoreduction pathway (i) can produce H_2O_2 by subsequent reaction of HO^{\bullet} in the absence of O_2 gas (Eq. 8).



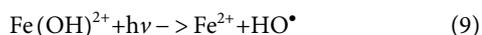
Photoreduction promotes the transfer of an e^- from DOM to the oxidized form of the metal (Fe, Mn, or Cu).



An e^- is transferred to molecular oxygen from the reduced metal.



Reduced metal reacts with hydroperoxyl radical, acidic conditions.



First hydrolysis product absorbs UV during photoreduction (Wang and Liu, 2014).

The simple act of heating water is reported to increase the production of ROS in some aqueous systems. Bruskov et al. (2002a,b) conducted experiments at 40°C in double distilled water and observed alternating production and decay of H_2O_2 over time. Kieber et al. (2014) noted that photoproduction rates of H_2O_2 from O_2 increase with increasing temperature from 0° to 35°C. Wilson et al. (2000b) conducted laboratory experiments with hot spring waters and found no statistical increase in H_2O_2 concentrations upon heating to 48°C in comparison with ambient laboratory temperatures over the same time interval. The

explanation for this discrepancy is not known although one could speculate that the difference in the ionic compositions of the experimental solutions could be a factor.

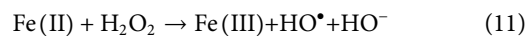
Minor amounts of H_2O_2 are also formed as a byproduct of microbial processes including nutrient acquisition, incomplete aerobic respiration, and photosynthesis (Moffett and Zafriou, 1990). While microbial production rates are slow compared to photochemical production rates, these pathways may be significant in dark conditions with abundant biomass.

Photodegradation through ROS production is a major pathway for decomposition of DOM (Eq. 10, Riedel et al., 2016). In the presence of soil-organic-matter extracts, oxalate-activated nanophase hematite generates ROS Eq. 10 (Huang et al., 2020), which are capable of remineralizing DOM to CO_2 (Eq. 10), as do other metal oxides (Blough and Zepp, 1995).

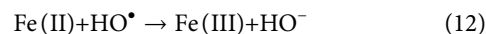


Degradation of DOM to low molecular weight (LMW) carbon coupled with mineralization (Huang et al., 2020).

Similarly, studies of aerosol chemistry demonstrate that iron oxide particulate matter aids photodegradation of H_2O_2 (e.g., Lin and Gurol, 1998). Johnson and Meskhidze (2013) found by modeling dissolved iron that both ferrous (Fe^{2+}) and ferric (Fe^{3+}) iron are capable of catalyzing the degradation of H_2O_2 . When Fe^{2+} is present, the Fenton reaction (Eqs. 11, 12) decays H_2O_2 (e.g., Bianco et al., 2020 and references therein) and, when Fe^{3+} is present, the Haber-Weiss mechanism (Eqs. 13, 14, which is restricted to oxygenic conditions) also occurs. Fe^{2+} reacts more readily with H_2O_2 than Fe^{3+} , so the Haber-Weiss reaction is insignificant in most cases (Zuo and Hoigne, 1992). Fenton decay is thought to be minimal in most natural waters, but it likely has a major role in metalliferous waters (Moffett and Zika, 1987; Zuo and Hoigne, 1992).



Step 1 of Fenton reaction.



Step 2 of Fenton reaction.



Haber Weiss reaction (Koppenol, 2001; Liovich and Fridovich, 2002).



Haber Weiss reaction alternative mechanism (Lin and Gurol, 1998).

Other elements, such as Cu and Mn, react directly with H_2O_2 to initiate decay (Eqs. 15, 16; see review by Bokare and Choi, 2014; Watts et al., 2005). The overall oxidation reaction of $M^{(n)+}$ with H_2O_2 goes through HO^{\bullet} in intermediate steps (e.g., Cu(I), Moffett and Zika, 1987) and increases pH while metal oxidation proceeds through HO_2^{\bullet} and its conjugate base $O_2^{\bullet-}$ and produces O_2 .

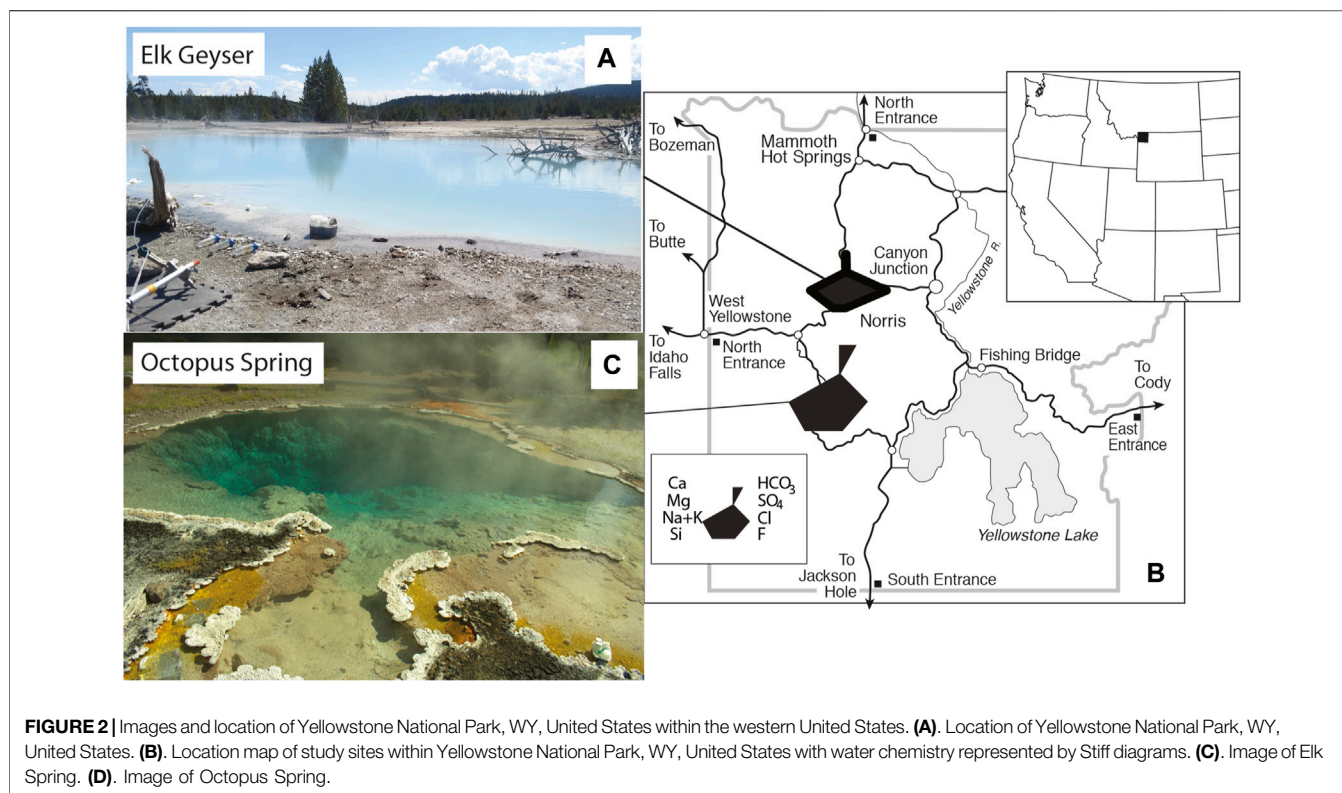
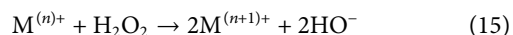
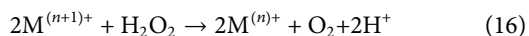


FIGURE 2 | Images and location of Yellowstone National Park, WY, United States within the western United States. **(A)**. Location of Yellowstone National Park, WY, United States. **(B)**. Location map of study sites within Yellowstone National Park, WY, United States with water chemistry represented by Stiff diagrams. **(C)**. Image of Elk Spring. **(D)**. Image of Octopus Spring.



Generic Fenton reaction.



Generic Haber Weiss reaction, alternative notation.

Biologic enzymes are major H_2O_2 sinks in low light and dark conditions, controlling H_2O_2 concentrations in the water column (Moffett and Zafiriou, 1990; Cooper et al., 1994). Some active bacteria and small algae (0.2–1.0 μm) release catalase and peroxidase enzymes as by-products of cell division and aerobic respiration but most importantly for catabolism of H_2O_2 (Brioukhanov et al., 2006). However, catalase and peroxidase are likely insignificant sinks of H_2O_2 in systems with low biomass, such as hydrothermal pools.

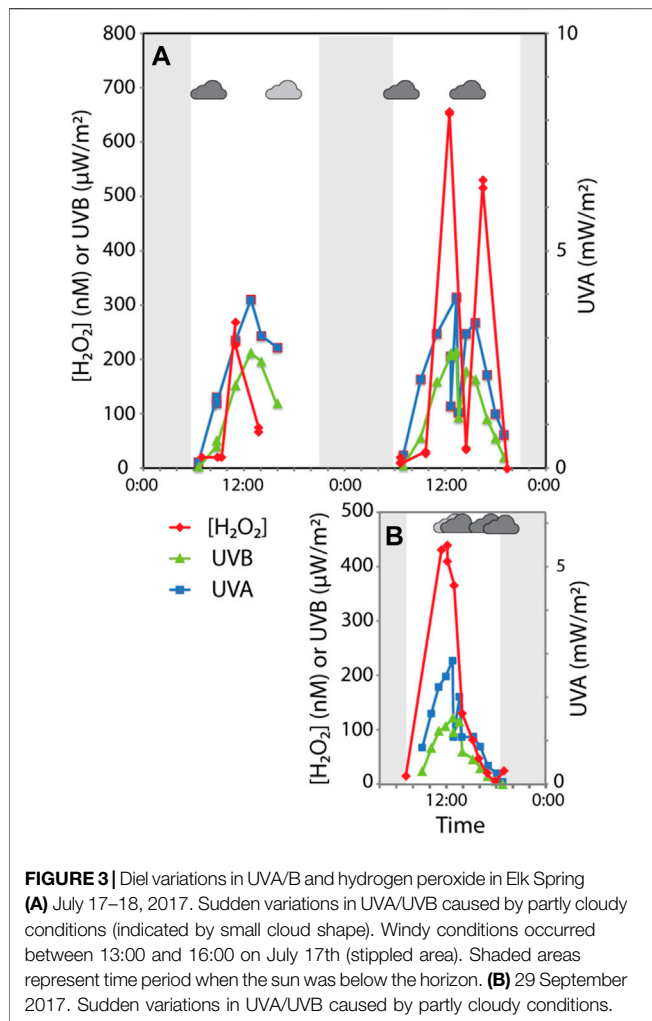
The chemical role of DOM in hot springs has only recently been investigated by new, high-resolution techniques (Rossel et al., 2015; Gonsior et al., 2018; Butturini et al., 2020). The development of high resolution mass spectrometry (HRMS) interfaced with soft-ionization techniques (e.g., electrospray) enabled the analyses of intact singly charged organic ions with unsurpassed mass resolution and allowed exact molecular formula assignments in complex DOM mixtures (Stenson et al., 2003; Koch et al., 2006). HRMS at high magnetic fields is a promising tool for advanced molecular characterization of dissolved organic matter (Kujawinski et al., 2004; Gonsior et al., 2009; Sleighter et al., 2009; Gonsior et al., 2011; Liu et al., 2011; Minor et al., 2012; Gonsior et al., 2013; Gonsior et al., 2014; Herzsprung et al.,

2017; Poulin et al., 2017; Kellerman et al., 2018; Powers et al., 2018; Hertzog et al., 2019; Roth et al., 2019; Zhao et al., 2019; Orrego-Ruiz et al., 2020) and has been recently applied to Yellowstone hot spring DOM (Gonsior et al., 2018). Gonsior et al., 2018 showed that each type of spring has specific DOM signatures associated with the water matrix that have been traditionally used to distinguish between hot spring types. Hence, a molecular comparison of different types of spring will showcase the stark differences in Yellowstone hot spring DOM (YDOM) between springs. This information will enable an initial evaluation of the potential role of DOM and underpin this study of ROS cycling in hot springs.

2 METHODS

2.1 Site Description

Yellowstone National Park (YNP), WY (**Figure 2**) is on a volcanic plateau in a region of crustal extension where active volcanism over the past 2.2 Ma is marked by three caldera-forming eruptions (Christiansen, 2001; Hurwitz and Lowenstein, 2014). Meteoric source waters from mountains in the northwest corner of the park flow through the subsurface along a complex system of fractures and faults into the Yellowstone caldera (Sorey, 1991). The shallow magma chamber heats ground water, which travels through the bedrock, dissolving silica, metals, and salts, and eventually migrates up conduits to emerge in areas of crustal weakness as hydrothermal features (Fournier, 1989; Hurwitz and



Lowenstein, 2014). These waters have variable compositions that change over time depending on temperature, lithology of contacted bedrock, fluid pressure gradients, and mixing between water types, among other factors. See Hurwitz and Lowenstein (2014) for additional background on the Yellowstone geothermal system.

Hot springs of interest consist of a vent, pool, and run-off channels. Vents are the primary source of heat and dissolved ions. Mixing is driven by both thermal convection and turbulence (Guidry and Chafetz, 2003). Waters in the pool and runoff channels cool, and consequently change composition, as a function of distance from the vent and discharge rate (de Wet and Davis, 2010). Springs of interest belong to the pond morphologic category and precipitate low relief rims of siliceous sinter and detrital material around a main pool (Guidry and Chafetz, 2003). We focused on the pools of two hot springs comprising a vent source with runoff channels for this study. Water in a pool has a longer residence time than water in vents or runoff channels and allows maturation of formation and degradation reactions to highlight photochemical processes; waters in vents and runoff channels have lower residence times.

The main water types found within the Yellowstone caldera are alkaline-chloride, acid-sulfate, and mixed (Fournier, 1989). Elk Spring ($T = 70.0\text{--}73.3^\circ\text{C}$, $\text{pH}=3.3\text{--}4.0$ at the sampling site), located near the Ragged Hills of Norris Geyser Basin (**Figure 2**), has an acid-chloride-sulfate water type (ACIS), defined as Type IIIa by White et al. (1988). Elk Spring (NRHA035) formed when the area known as “The Gap” heated up in 2000–2002 (Shean, 2006; Yellowstone RCN, <http://rcn.montana.edu/Features/Detail.aspx?id=6995>, accessed 12–26-2020; 44.72954N, 110.712W). This water type is the result of mixing of chloride- and silica-rich waters with dilute, acidic, meteoric waters. This water type is common in the Norris Geyser Basin, and its acidic pH commonly results in high metal concentrations. Gardner et al. (2011) defined the end member water sources in this area. These include: 1) old thermal waters that circulate deep beneath the surface whose chemistry is dominated by high-temperature water-rock interactions and 2) young cold waters that circulate through a shallow, high porosity Quaternary-age siliceous volcanic aquifer whose chemistry is dominated by low-temperature silicate weathering. Young, cold waters source cold springs ($<20^\circ\text{C}$), while older, mineral-rich waters source hydrothermal waters ($>50^\circ\text{C}$).

Elk Spring was selected as the primary study site due to its high Fe concentrations (**Table 2**) when compared to alkaline-chloride type springs (i.e., AlkCl, Type I of White et al., 1988). This water type is a mixture of two end member water types: acid-sulfate (Type IIb of White et al., 1988) and alkaline-chloride (Type I of White et al., 1988). Although ACIS springs are less common than alkaline-chloride and acid-sulfate springs, they are ideal targets for this study because they have reasonable dissolved metal concentrations, high silica concentrations, low pH, and reasonable clarity. This water should also have a high preservation potential due to the presence of dissolved metals and Si concentrations. This study is the third report of H_2O_2 concentrations in acidic, Fe-bearing hydrothermal systems (Mesle et al., 2017; Wilson et al., 2000a). Octopus Spring ($T=88.7\text{--}90.4^\circ\text{C}$, $\text{pH}=7.8\text{--}8.1$; Yellowstone RCN, <http://rcn.montana.edu/Features/Detail.aspx?id=5609>, accessed 12–14-2020; 44.53408N, 110.7979W) was selected for use in comparison, photochemical studies due to its AlkCl water type (**Table 2**). This AlkCl water type is more widely represented in YNP than the ACIS type waters, but both have a high potential for biomarker preservation. Excitation-emission matrices (EEM) were reported for both Elk Spring and Octopus Spring in Gonsior et al. (2018). These EEMs further highlight differences in these water types, along with their low CDOM contents. While laboratory experiments could be repeated on both water types, *in situ* H_2O_2 could only be measured at Elk Spring. It remains unclear why attempts to measure H_2O_2 *in situ* with the scopoletin-horseradish peroxidase method used here were unsuccessful in Octopus Spring. The starting fluorescence was above the working range of the spectrofluorometer, and the sample was diluted with H_2O_2 -free MilliQ water to reduce the fluorescence. Scopoletin suppressed the fluorescence in the next step instead of enhancing it as is expected (Holm et al., 1987). This experiment was repeated several times, and the results indicated either some deactivation of the scopoletin by an

TABLE 2 | Hot spring water compositions.

Analyte	Elk pool		Octopus spring		Purple pool
	July	September	July	October	October
Temperature (°C)	71.5–73.3	70.0	88.7–90.4	89.5	90.0
pH	3.93–4.20	3.31	7.82–7.95	8.06	7.85
Alkalinity (mg/L)	4.1	-	270.4	268.8	177.6
H ₂ O ₂ (nM)	<20–652	<20–443	-	-	-
Dissolved Oxygen (mg/L)	-	1.5	-	6.1	4.0
Total soluble iron (mg/L)	<0.1–0.35	<0.1–0.35	-	-	-
Total soluble iron (mg/L)	<0.2	1.2	-	<0.2	<0.2
Nitrate (mg/L)	-	0.09	-	0.10	0.10
Nitrate ^a (mg/L)	<0.1	<0.1	0.1	0.2	<0.1
Ammonia (mg/L)	0.10–0.32	0.25	2.26	1.01	0.36
Sulfide (mg/L)	<0.001	-	0.17 ^b	-	-
Fluoride ^a	8.8	3.5	29.0	7.9	6.3
Chloride ^a	736.0	633.3	262.8	266.4	159.2
Sulfate ^a	66.4	108.6	20.4	19.5	17.3
Potassium ^c (mg/L)	56	50	-	14	18
Manganese ^c (mg/L)	<0.04	<0.04	-	<0.04	0.08
Sodium ^c (mg/L)	399	390	-	287	183
Silica ^c (mg/L)	167	148	-	131	103
DOC (µg/L)	-	571 ± 8	-	253 ± 13	-
SPE-DOC (µg/L)	-	144 ± 0.3	-	11.3 ± 0.2	-
DOC extraction efficiency	-	25 ± 4%	-	4 ± 1%	-
SPE-DOS (µg/L)	-	3.56 ± 0.06	-	0.56 ± 0.02	0.520 ± 0.002
SPE-DOC:DOS (molar ratio)	-	108 ± 2	-	54 ± 2	-

^aMeasure on IC.

^bJuly 2006 data. Values with reported error are averages ± range/2.

^cMeasured on ICP-OES, by SGS, Canada.—data not collected.

unknown component or immediate absorbance of the fluorescence by CDOM. However, an unstable constituent undoubtedly causes the interference because H₂O₂ could be measured in samples from the spring after 3 h.

2.2 Sampling Schedule

H₂O₂ and UV were measured from sunrise to sunset on July 17–18, 2017 and 30 September 2017 (SI). UVA (315–400 nm) and UVB (280–315 nm) irradiance were measured by radiometers, zeroed before each use (International Light (Newburyport, Maine) IL-Radiometer with SED 240/UVB-1/W (265–310 nm) and SED 033/UVA/W (330–375 nm) detectors). H₂O₂ samples were collected ~4 h apart, but sample frequency varied based on weather and time constraints. Samples were not collected overnight for safety reasons and because previous studies showed that, under dark conditions, H₂O₂ concentrations drop below the detection limit (Wilson et al., 2000a).

Water samples were all collected from shallow surface waters where photochemical reactions are rapid. All samples from a given spring were collected at the same location for consistency.

2.3 Hydrothermal Spring Sample Collection and Characterization

Detailed methods for sample collection and field analyses are in **Supplementary Information S1.1**. Samples were collected and stored as outlined in **Supplementary Table S2.1** and analyzed according to methods in **Supplementary Table S2.2**.

2.4 Hydrogen Peroxide Analysis by the Scopoletin Fluorescence Quenching Method

H₂O₂ was measured using a modification of scopoletin fluorescence-quenching method (Holm et al., 1987; Zhang and Wong, 1999; Wong et al., 2015). Fluorescence was measured using a customized setup from Ocean Optics (Largo, FL) with a LED light source (LLS-385), sliding linear variable emission filter set to 460 nm, and the Maya LSL spectrophotometer. Plastic cuvettes (Thermo Scientific) with a 220–900 nm passable wavelength were used. Samples were pipette-mixed in the cuvettes both in the field and in the laboratory prior to insertion into the cuvette holder. Additional details are in **Supplementary Information S1.2**.

2.5 Ultrahigh resolution Mass Spectrometry Analysis of Yellowstone Hot Spring Dissolved Organic Matter

YDOM was solid-phase extracted (SPE) from Octopus Spring and Elk Spring in fall 2017. 20 L of spring water was acidified to pH 2 using HCl (32%, Sigma Aldrich) and then gravity-fed through a 1g Agilent Bond Elut PPL cartridge (Agilent Bond Elut, 1g PPL resin, 6 ml barrel volume). After extraction, the cartridge was rinsed with 10 ml of 0.1% formic acid water (Chromasolv, LC-MS grade 0.1% formic acid) and then eluted with 10 ml pure methanol (Chromasolv, LC-MS grade methanol). Samples were then stored at –20 C in the freezer prior to analysis.

All YDOM samples were analyzed using a Bruker Solarix 12 T Fourier transform ion cyclotron resonance (FT-ICR) MS. Electrospray ionization was applied in negative ion mode to generate largely intact singly charged ions. Additional information about the FT-ICR MS technique is given elsewhere (Hertkorn et al., 2007). Briefly, YDOM methanolic extracts were directly injected using an autosampler at a flow rate of 0.3 $\mu\text{L}/\text{h}$ and 500 scans were averaged at a time domain of 4 megawords. External pre-calibration prior to mass spectrometric analyses was undertaken using arginine cluster standards. To further enhance the precision, post-calibration was performed using internal standards of high relative abundance exact mass peaks with known molecular formulae. The reproducibility of the SPE method in conjunction with the same mass spectrometer used in this study has been previously described on triplicate samples (Shakeri Yekta et al., 2012). The achieved mass accuracy of less than 200 ppb allowed exact molecular formula assignments based on a complex array of atoms typically associated with DOM and the molecular formula assignments are based on the following elements: $^1\text{H}_{0-∞}$, $^{12}\text{C}_{0-∞}$, $^{16}\text{O}_{0-∞}$, $^{32}\text{S}_{0-10}$, $^{14}\text{N}_{0-5}$, as well as the isotopologues $^{13}\text{C}_{0-1}$ and $^{34}\text{S}_{0-1}$.

2.6 Dissolved Organic Sulfur in SPE-YDOM

DOS was determined for SPE-YDOM samples following established methods (Ksionzek et al., 2016; Ossola et al., 2019) using a Triple Quadrupole inductively coupled plasma-mass spectrometer (ICP-MS/MS, Agilent 8900 ICP-QQQ) equipped with a collision/reaction cell. To improve sulfur detection and minimize interferences, oxygen gas was reacted with sulfur to form $^{32}\text{S}^{16}\text{O}$ in the collision cell. Sulfur was determined using m/z 32 (MS1) and m/z 48 (MS2) with an integration time of 0.5 ms, 1 point per peak, 3 replicates and 50 sweeps per replicate. The ICP was tuned weekly using a multi-element tuning solution containing Li, Co, Y, Tl, and Ce (Agilent) diluted to $1\ \mu\text{g}\ \text{L}^{-1}$ with pure water. SPE-YDOM samples were prepared by drying aliquots of the methanolic extracts under N_2 and redissolving them in a 100–1000x dilution of ultrapure water. ^{59}Co (Agilent) was used as an internal standard in all samples, blanks, and standards and diluted to final concentration of $0.5\ \mu\text{g}\ \text{L}^{-1}$. S standard curves were prepared from 0 to 50 ppb using dilutions of a 10 ppm multi-element calibration mix (Agilent) and were in agreement to those made using dilutions of $\text{Na}_2\text{S}_2\text{O}_3$ (>99.99% trace metal basis, Sigma-Aldrich). A sulfur containing organic compound (3-chloro-4-(sulfonyl) thiophene-2 carboxylic acid, Sigma-Aldrich) was also analyzed to assess the accuracy of sulfur determination and was within 5% of expected concentration. All final DOS values are corrected for dilution and extraction volumes noted above.

2.7 Excitation-Emission Matrix Spectroscopy

SPE-YDOM samples for optical property analysis were prepared at higher concentrations than described above, by drying methanolic extracts and re-dissolving them in a 40x dilution of ultrapure water. Dissolved organic carbon (DOC)

concentrations for SPE-YDOM samples were determined using a Sievers 5310C TOC analyzer calibrated with potassium hydrogen phthalate standards between 0.05 and $50\ \text{mg}\ \text{C}\ \text{L}^{-1}$. CDOM absorbance spectra ($A(\lambda)$) and EEM fluorescence spectra were measured using an Aqualog spectrofluorometer (Horiba). $A(\lambda)$ spectra were collected at 1 nm intervals between 240 and 750 nm. Excitation was scanned at 3 nm intervals between 240 and 550 nm and emission spectra were collected at fixed 3.26 nm intervals between 250 and 600 nm. Ultrapure water served as the absorbance and fluorescence blank. Absorbance was corrected for any offsets between samples and blank and/or instrument drift by subtracting all spectra by average absorbance between 680–720 nm. Absorbance spectra normalized to DOC concentration and spectrophotometer cell pathlength (0.01 m) are reported as $a(\lambda)/[\text{DOC}]$ ($\text{L}\ \text{mg}^{-1}\ \text{m}^{-1}$) here. EEM spectra were corrected for Rayleigh scattering following an established method (Zepp et al., 2004) and were normalized to the emission area of a the water Raman scattering peak at an excitation of 350 nm. Thus, fluorescence intensities reported here are expressed water Raman units (RU).

2.8 Experimental Design

Experiments in the field and the laboratory were conducted with hot spring water, which was treated in various ways for field and laboratory experiments, as described below (**Supplementary Table S2.3**). H_2O_2 concentrations from field experiments were compared with *in situ* values for Elk Spring; *in situ* values could not be measured for Octopus Spring most likely because of interaction between scopoletin and an unknown component in Octopus Spring water. This interaction ceased within 24 h after collection, and we were able to measure H_2O_2 concentrations in laboratory experiments with Octopus Spring water.

2.9 Field Experimental Setup

100 ml of freshly collected waters placed in UV permeable polyethylene Whirlpak® bags or UV-permeable Fisherbrand™ 50 ml centrifuge tubes according to the conditions of the experiments (filtered, unfiltered, Fe added, F^- added). Bags were floated in the spring near the sampling site to mimic spring temperatures and UVA/B irradiance. MilliQ and dark (covered in aluminum foil) controls were included and sampled along with experiments. The temperature and pH were measured at the start and end of each experiment. Particulate matter was removed in selected field experiments using $0.2\ \mu\text{m}$ Thermo Scientific Target 2 brand nylon filters. In this paper, “unfiltered” means that both particulate and soluble materials were present, while “filtered” means that particulate matter ($<0.2\ \mu\text{m}$) was removed. Fe was added to select field experiments in the form of sterile, synthetic Fe and colloidal Si-coated petrographic slides added to polypropylene centrifuge tubes and incubated next to the hot spring. Rates were calculated as the concentration of H_2O_2 at time, t , divided by time per incident radiation (W/cm^2). Additional details are in S1.3.

2.9 Laboratory Experimental Setup

Laboratory experiments were conducted in acid-washed porcelain dishes in a dark laboratory cabinet to block external irradiation. H_2O_2 formation studies were irradiated by constant UVA/B irradiance from linear fluorescent lamps for 4 h; the experiments were arranged in a single line beneath the light source. Bulbs emitted $760\text{--}772 \mu\text{W}/\text{cm}^2$ UVA and $0.73\text{--}1.02 \mu\text{W}/\text{cm}^2$ UVB as measured at sample height with an International Light Technologies IL1400A m (International Light Technologies, Peabody, MA). Waters used in the experiments were collected during fieldwork and kept in cool, dark conditions; the volume of water collected for the experiments was limited by NPS collection permit. In experiments, 100 ml of water were altered according to experiment conditions (filtered, unfiltered, or addition of $\text{Fe} \pm \text{F}$, catalase, or SOD) and added to porcelain dishes. H_2O_2 , temperature, and pH were always measured at the start and end of each experiment. Fe , F^- , superoxide dismutase (SOD), and catalase amendments were added to experimental solutions to test their effects on H_2O_2 production rates. Fe was added in the form of sterile, synthetic Fe and colloidal Si-coated petrographic slides.

Geochemical speciation was modeled with PHREEQC (Parkhurst and Appelo, 1999). Rates were calculated as the difference between the starting and final H_2O_2 concentrations at time, t , divided by the time interval and incident radiation (W/cm^2). Additional details are in S1.4.

3 RESULTS

Laboratory analyses and field analyses were used to characterize Elk Spring and Octopus Spring compositions in July and September 2017 (Table 2).

Elk Spring (ACIS + Fe) had a temperature range of $71.5\text{--}73.3^\circ\text{C}$ and a pH range of $3.9\text{--}4.0$ over the course of the study. Alkalinity was <0.1 meq/L in Elk Spring due to the low pH. Field analyses showed $<18\text{--}72 \mu\text{M}$ Fe(II) and $55\text{--}165 \mu\text{M}$ NH_4^+ , NO_3^- and S^{2-} concentrations were below detection. Chloride dominated anions with a smaller amount of SO_4^{2-} present. Sodium dominated cations with lesser amounts of potassium and calcium. Transition elements (other than Fe) were below detection by ICP-OES. Dissolved organic carbon and total dissolved nitrogen contents were low: 0.57 ± 0.01 and 0.41 ± 0.01 mg/L, respectively.

Octopus Spring (AlkCl) had a temperature range of $88.7\text{--}90.4^\circ\text{C}$ and a pH range of $7.8\text{--}8.0$ over the course of the study. Alkalinity was 5.4 meq/L. Field analyses showed $130 \mu\text{M}$ NH_4^+ , NO_3^- concentration was $16 \mu\text{M}$ in field and $32 \mu\text{M}$ in lab analyses. Historic S^{2-} concentrations were 0.002 and $0.17 \mu\text{M}$ (Ball et al., 2010; Hinman, unpubl, 2006). Chloride dominated anions with a smaller amount of SO_4^{2-} present. Sodium dominated cations with lesser amounts of potassium and calcium. Transition elements were below detection by ICP-OES. Dissolved organic carbon and total dissolved nitrogen contents were low: 0.25 ± 0.01 and 0.03 ± 0.01 mg/L, respectively.

3.1 Diel Field Study

UV flux varied throughout sampling periods due to the solar cycle and to weather (i.e., wind, local cloud cover). H_2O_2

concentrations follow UVA and UVB trends, as is apparent on July 18 when peaks of H_2O_2 closely follow peaks in UV (Figure 3). Maximum H_2O_2 concentrations were reached around noon. On all occasions, a thick layer of steam covered Elk Spring in the early morning time (Supplementary Table S2.4). Maximum UVA intensities reached close to $4 \text{ mW}/\text{cm}^2$ on both days in July but only $2.89 \text{ mW}/\text{cm}^2$ in September (Supplementary Table S2.4). *In situ*, bag, and tube experiments were subjected to the same UV flux on July 18th. Supplementary Table S2.5 provides a snapshot of the H_2O_2 formation rate in the hot spring compared to those after 4 hours in bag experiments.

3.2 In Situ H_2O_2 Production Experiments

Average *in situ* H_2O_2 concentrations in Elk Spring were 76 nM, 217 nM, and 158 nM for July 17th, July 18th, and September 29th, respectively (Figure 3; Table 3, Supplementary Table S2.4). Maximum H_2O_2 concentrations were 284 nM, 644 nM, and 431 nM for July 17th, July 18th, and September 29th, respectively. July 17 had the lowest H_2O_2 concentrations despite having similar maximum UV flux as July 18 and a much higher UV flux than September 29 (Table 3). Heavy cloud cover and high winds were observed on July 17 and the other study days (Supplementary Table S2.6). H_2O_2 peaks were reached between 11:00 a.m. and 12:30 on all occasions (Figure 3, Supplementary Table S2.7).

3.3 Results From Field Experiments

H_2O_2 concentrations varied in the field between *in situ* measurements and bag experiments (Table 3, Supplementary Tables S2.5, S2.7, S2.8). The bag experiments tested the effects of filtration on H_2O_2 formation rates. Specifically, the highest H_2O_2 concentrations were measured *in situ* in Elk Spring, followed by rates for filtered waters, and then rates for unfiltered waters. Dark controls had H_2O_2 concentrations below detection at the end of the experiment. Between 13:30 and 14:30, intermittent cloud cover decreased incident UV intensity, and *in situ* H_2O_2 concentrations were lower (33 nM) but recovered by the following time point (525 nM at 16:30). H_2O_2 concentrations in bag experiments at 16:30 were much lower than values at 12:30. The recovery of H_2O_2 concentrations *in situ* suggests continuation of formation and decay mechanisms in the spring. Low H_2O_2 concentrations in bag experiments after a period of cloudiness suggests inactivation of the H_2O_2 formation mechanism. At 19:30, all waters were below the detection limit (~ 20 nM) due to low UV irradiance.

The difference between the H_2O_2 concentrations in Elk Spring and tube experiments was even greater. Tube experiments were designed to test the effect of increasing Fe concentration on H_2O_2 formation rates. Rates in tubes were less than half those observed *in situ*.

3.4 Impact of Fe Speciation

H_2O_2 formation rates were higher regardless of hot spring composition in experiments with added Fe^{3+} -

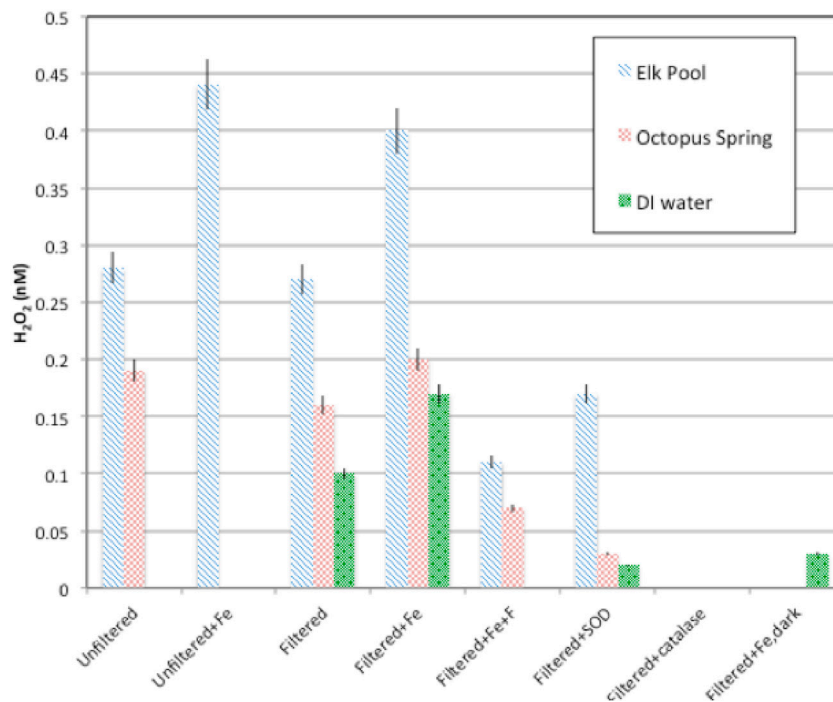


FIGURE 4 | H₂O₂ production rates for particulate and dissolved hot spring waters with or without amendments (Fe-oxyhydroxide), SOD, catalase). In all cases, formation rates in Elk Spring waters were higher than those in Octopus Spring water.

TABLE 3 | Summary of results from field experiments.

Container	Amendment	pH	Fe Average	Formation rate ^a	UVA + UVB
			mg/L	(nM/W/s/cm ²)	(mW/cm ²)
Elk Spring, Filtered	<i>in situ</i>	4.2	0.35	207.2 ± 4.3	3.083
Filtered	bag	None	na	188.1 ± 4.0	
Unfiltered	bag	None	na	27.2 ± 0.4	
Filtered, dark	bag	None	na	-	
Unfiltered, dark	bag	None	na	-	
Elk Spring, Filtered	<i>in situ</i>	4.2	0.35	220.7 ± 4.5	3.385
Filtered	tube	Fe	3.9	91.0 ± 3.4	
Unfiltered	tube	Fe	4.9	87.0 ± 1.6	
MilliQ	tube	Fe	3.6	3.79	-
Filtered MilliQ, dark	tube	Fe	3.9	1.63	-

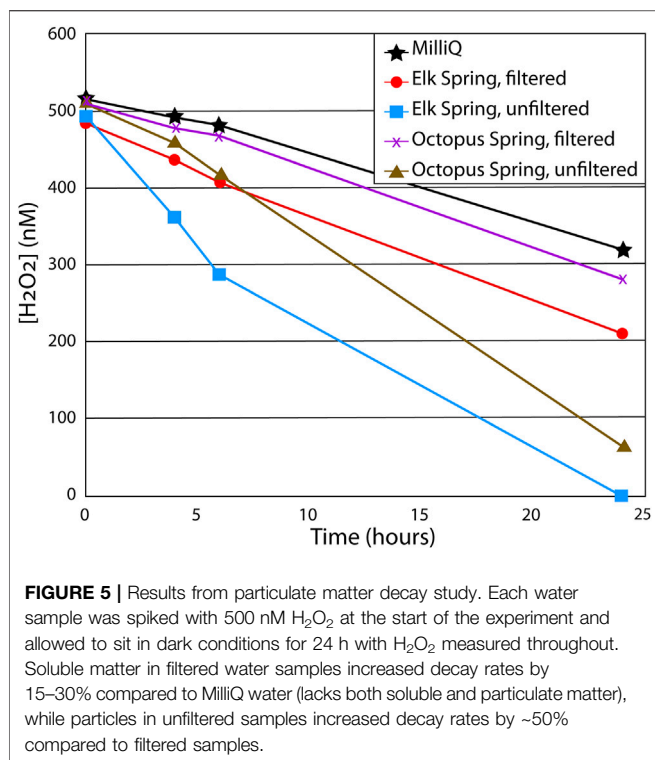
^aFormation rates were calculated as the difference between the starting and final H₂O₂ concentrations at time, t, divided by the time interval and incident radiation (W/cm²). Additional details are in **Supplementary Information S1.4**. na = not analyzed. - = rate could not be calculated because the final concentration was below the detection limit (20 nM). Values with reported error are averages ± range/2.

oxyhydroxide in both the field (Table 3, Supplementary Tables S2.5, S2.7, S2.8) and laboratory (Figure 4; Table 4, Supplementary Table S2.9). Natural water chemistries had faster formation rates compared to MilliQ, although a small amount of H₂O₂ was produced in MilliQ experiments with Fe added in dark conditions (Table 4).

Elk Spring experiments had the fastest formation rates regardless of experimental conditions. The addition of F⁻ decreased H₂O₂ formation rates in Fe-enriched experiments (Figure 4, Supplementary Table S2.5). Specifically, the H₂O₂

formation rate in Elk Spring-Fe-F⁻ experiments was ~73% slower than in Fe-added experiments without F⁻. Soluble Fe (II) and pH increased in Elk Spring-Fe-F⁻ experiments compared to experiments without F⁻.

The formation rate in Octopus Spring-Fe-F⁻ experiments was ~65% slower than in Fe-added experiments (Figure 4, Supplementary Table S2.9). Octopus Spring-Fe-F⁻ experiments had a pH 0.33 lower and a total, soluble Fe ~0.005 mM higher compared to Octopus Spring-Fe experiments. However, concentrations of total Fe in



Octopus Spring experiments without added Fe were below detection by the Ferrozine method (<36 μM; Lovley and Phillips, 1987) and could not be monitored. Other transition elements known to react with ROS were below

detection (Cu, 0.002 mM and Mn, 0.0007 mM by ICP-AES) in both Octopus and Elk Springs.

3.5 Effects of Superoxide Dismutase and Catalase

The addition of SOD decreased H₂O₂ formation rates, but did not completely stop H₂O₂ production indicating that some production proceeds by reductive pathways not involving superoxide dismutation (Figure 4; Table 4, Supplementary Table S2.9). SOD decreased formation rates by 35% (0.10 nM/W/sec/m²) in Elk Spring experiments, 76% (0.11 nM/W/sec/m²) in Octopus Spring experiments, and statistically 100% (0.11 nM/W/sec/m²) in MilliQ, and all experiments experienced an increase in pH when SOD was added. The pH also increased in experiments without SOD, but to a lesser extent.

As expected, H₂O₂ concentrations were below detection in all experiments with added catalase, and all experiments experienced an increase in pH. (Figure 5; Table 4, Supplementary Table S2.9).

3.6 Effects of Particulate Matter on H₂O₂ Formation and Decay Rates

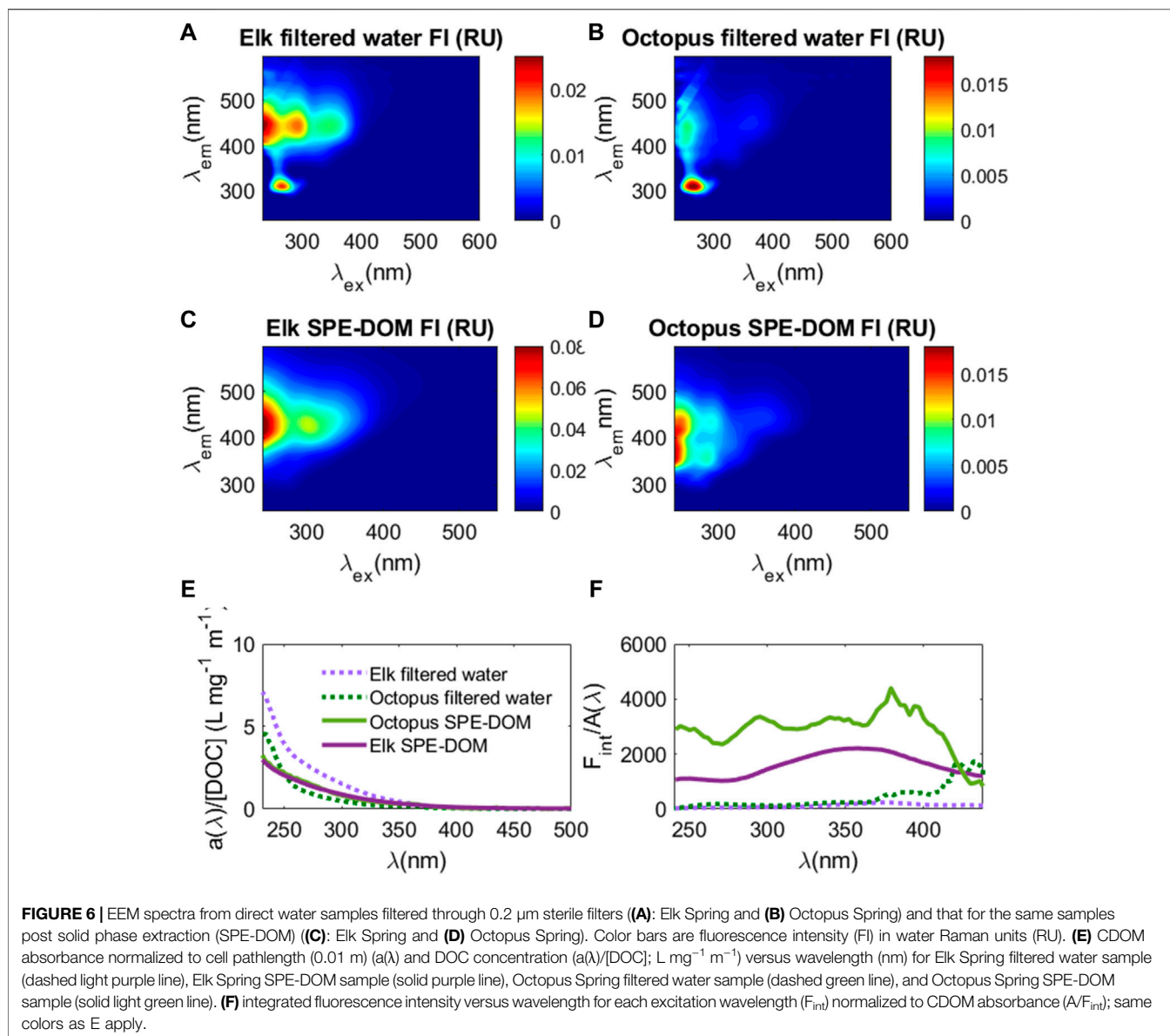
Both field and laboratory studies were conducted to assess the role of particulate matter on H₂O₂ formation and decay rates by comparing H₂O₂ production using filtered and unfiltered spring waters. Laboratory experiments showed that particulate matter had mixed effects on H₂O₂ formation rates compared to those without particles under constant UV irradiance, regardless of water composition (Figure 5; Table 4, Supplementary Table

TABLE 4 | Experimental conditions and formation rates for laboratory experiments.

Solution	Filtered	Condition	[Fe] Start	[Fe] End	Formation rate ^a (nM/W/Sec/m ²)
MilliQ	Yes		<0.2	<0.1	0.132 ± 0.022
MilliQ	Yes	Fe	<0.2	0.8	0.166 ± 0.006
MilliQ	Yes	Fe, dark	<0.2	<0.1	0.027 ± 0.006
MilliQ	Yes	catalase	<0.2	na	<0.018
MilliQ	Yes	SOD	<0.2	na	<0.018
Octopus Spring	Yes		<0.2	0.074	0.161 ± 0.018
Octopus Spring	Yes	Fe	<0.2	0.052	0.202 ± 0.024
Octopus Spring	Yes	Fe,F	<0.2	0.924	0.065 ± 0.006
Octopus Spring	Yes	catalase	<0.2	na	<0.018
Octopus Spring	Yes	SOD	<0.2	na	0.030 ± 0.002
Octopus Spring	No		<0.2	na	0.187 ± 0.007
Elk Spring	Yes		0.26	0.405	0.265 ± 0.013
Elk Spring	Yes	Fe	0.26	0.902	0.411 ± 0.005
Elk Spring	Yes	Fe,F	0.26	0.383	0.113 ± 0.005
Elk Spring	Yes	catalase	0.26	na	<0.018
Elk Spring	Yes	SOD	0.26	na	0.170 ± 0.013
Elk Spring	No		0.26	na	0.284 ± 0.006
Elk Spring	No	Fe	0.26	1.1	0.435 ± 0.035
Elk Spring	No	dark	0.26	na	<0.018
Purple Pool	Yes		<0.2	na	0.167 ± 0.014
Purple Pool	No		<0.2	na	0.277 ± 0.011

UVA + UVB = 0.77 mW

^aFormation rates were calculated as the difference between the starting and final H₂O₂ concentrations at time, t, divided by the time interval and incident radiation (W/cm²). Additional details are in **Supplementary Information S1.4**. na = not analyzed.



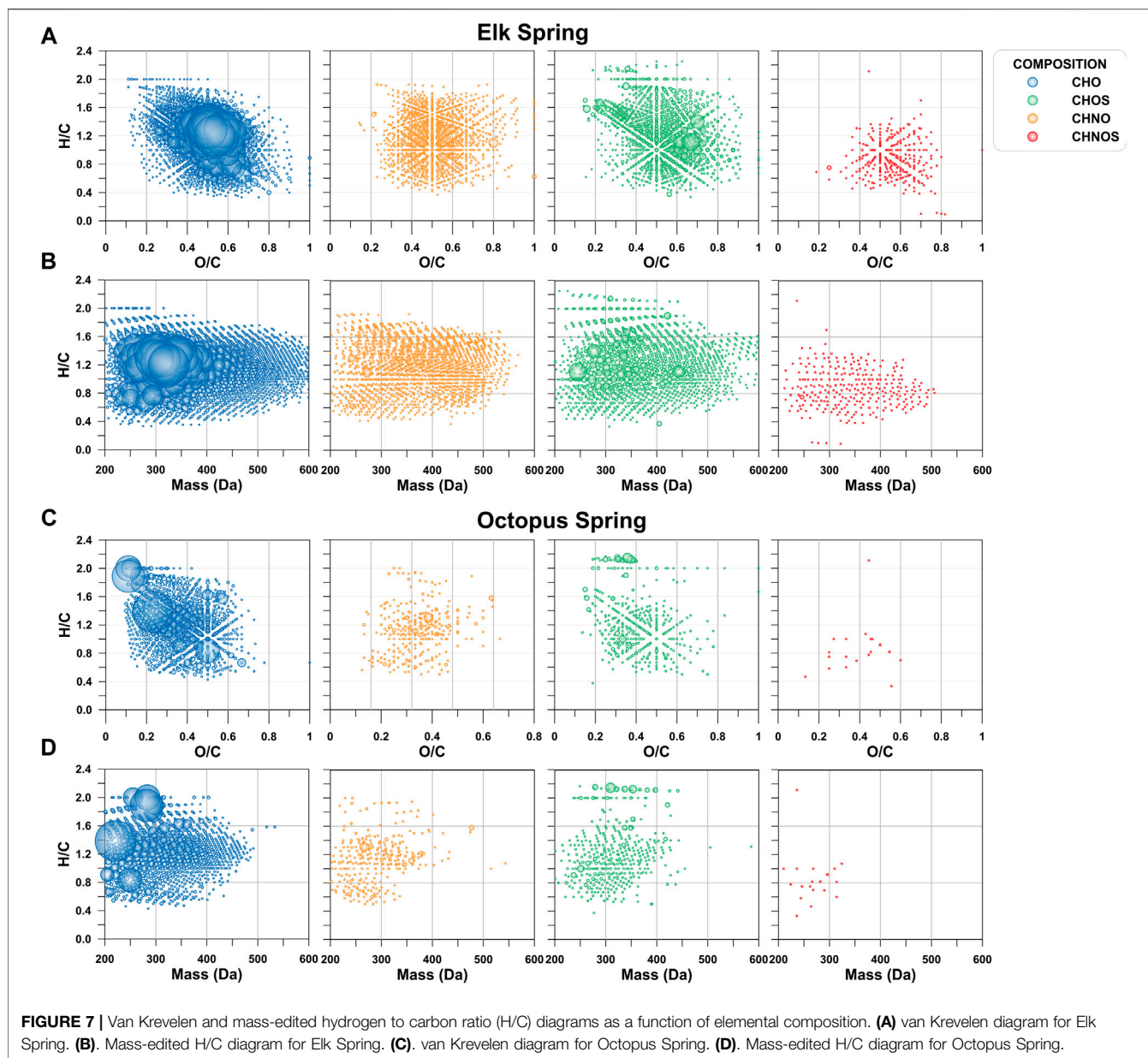
S2.9). Specifically, the presence of particles showed no effect on H_2O_2 formation rate within experimental error in the case of the Elk Spring water but increased the rate by 16% in Octopus Spring water type in laboratory experiments. The effect of particles on the rate increase was greater for Octopus Spring than for Elk Spring. In contrast, field experiments at Elk Spring yielded comparable formation rates *in situ* and for bag experiments with filtered water, which were both higher than for unfiltered experiments (**Table 3, Supplementary Table S2.5**). These results showed that dissolved components were primarily responsible for H_2O_2 formation in both Elk Spring and Octopus Spring, as previously suggested by Wilson et al. (2000a), but that particles were capable of contributing to H_2O_2 formation as well in Octopus Spring.

Results from the dark decay laboratory studies showed that H_2O_2 decay rates were faster in the presence of particulate

matter (i.e., unfiltered waters) (**Figure 5**). Furthermore, ACIS, Fe-bearing type Elk Spring (**Supplementary Table S2**) always had faster decay rates compared to AlkCl, metal-poor type Octopus Spring (**Table 2**). Both natural hydrothermal water samples had faster decay rates compared to the MilliQ control (lacked both particulate and dissolved matter). These results suggest that particulate matter played a primary role and dissolved matter a secondary role in H_2O_2 decay, while dissolved Fe appeared to further increase decay rates.

3.7 Molecular and Optical Characterization of Hot Spring Dissolved Organic Matter

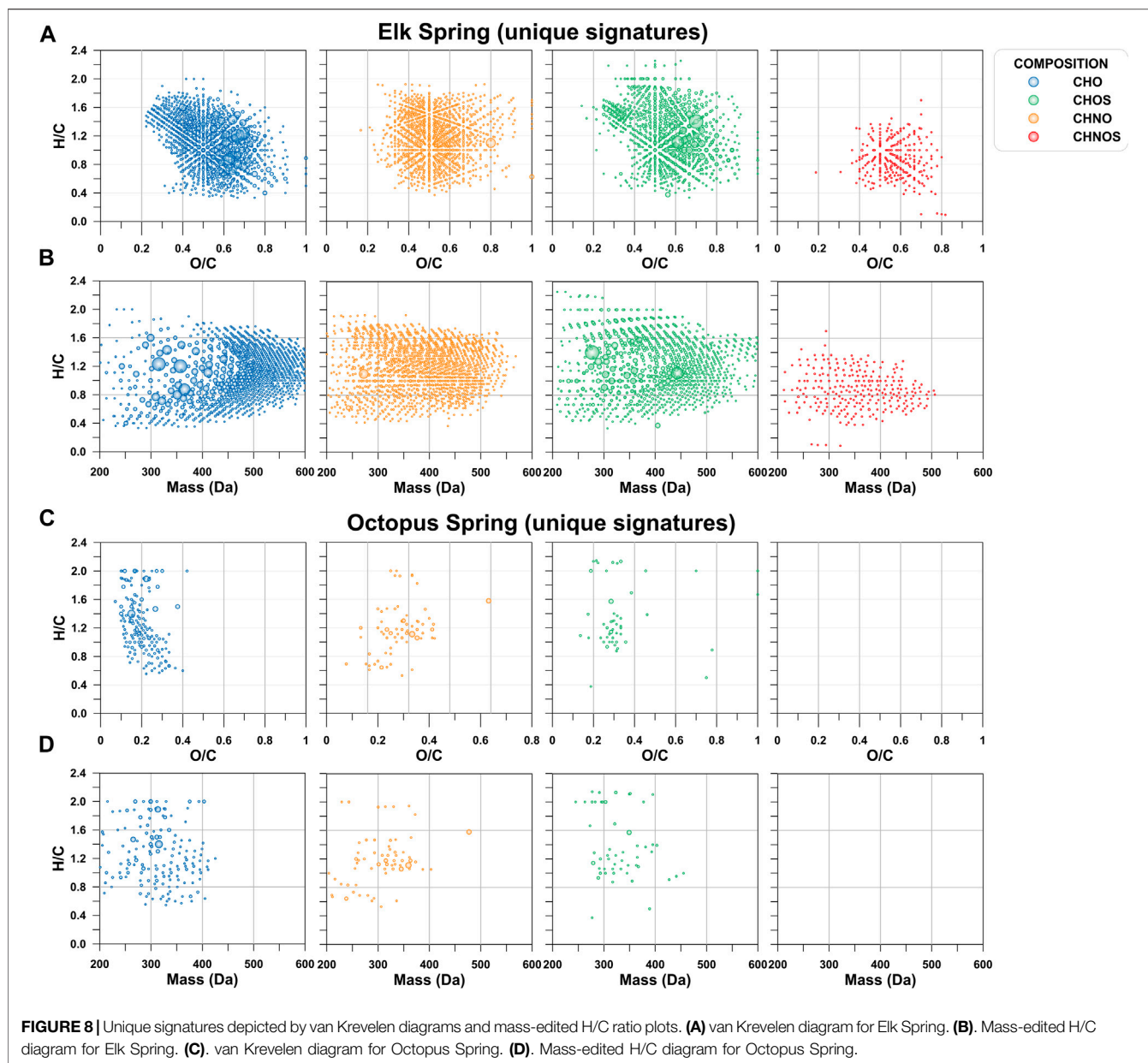
While DOC extraction efficiencies are typically 40–60% using the SPE technique in marine and freshwaters (Dittmar et al., 2008),



DOC extraction efficiency was $25 \pm 4\%$ at Elk Spring and only $4 \pm 1\%$ at Octopus Spring. Despite low extraction efficiencies, because iron is known to enhance absorbance values and potentially quench fluorescence values (Weishaar et al., 2003; Poulin et al., 2014), SPE allows for evaluation of these parameters without (or minimal) interferences. Octopus Spring had a much lower absorbance spectrum when compared to Elk Spring, but when normalized to DOC concentrations ($a(\lambda)/[\text{DOC}]$), absorbance spectra were very similar in magnitude and shape between these two samples (Figure 6). Despite these similarities in absorbance, EEM spectra showed distinct differences between samples and post-extraction. After extraction, the Elk Spring SPE-YDOM EEM spectrum had higher fluorescence intensities than before extraction and

resembled the broad fluorescence spectrum typical of oxygenated freshwater samples (Figure 6). Octopus Spring, on the other hand, had similar fluorescence intensities before and after extraction, but higher fluorescence in the excitation/emission (ex/em) range of 240–320 nm/310–500 nm. There were also a few distinct fluorescence “peaks” (i.e., areas with high fluorescence) in the Octopus Spring SPE-YDOM sample around ex/em regions of ~ 250 nm/350 nm, 250 nm/420 nm, 280 nm/350 nm and 280 nm/420 nm.

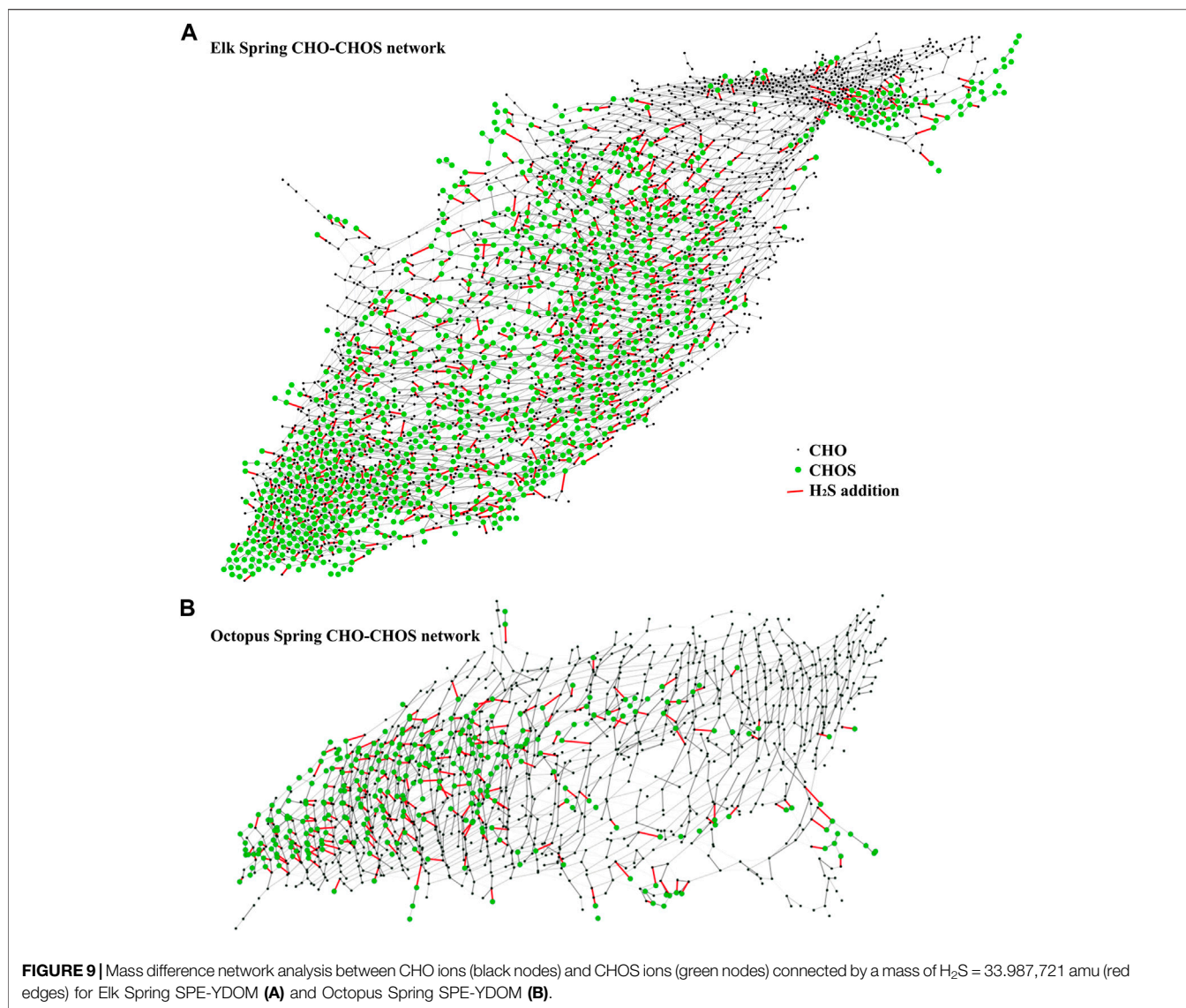
Even though a large portion of the DOC pool was missed by the extraction technique used here, and only what was visible in negative mode ESI is described here, FT-ICR MS results showed a large diversity of molecular signatures in the SPE-YDOM pools of Elk and Octopus Springs (Figure 7). Elk Spring had a much larger



diversity of DOM signatures with generally higher molecular weight and high O/C ratios when compared to Octopus Spring. On the other hand, low molecular weight (<450 Da) signatures of low (<0.6) O/C ratios dominated YDOM in Octopus Spring. A detailed analysis of the unique signatures in each spring revealed even more the fundamental differences between these two springs (**Figure 8**). In line with lower extraction efficiencies, there were far fewer unique molecular ions at Octopus Spring when compared to Elk Spring. Elk Spring also had a larger diversity of ions containing nitrogen and/or sulfur. We were not able to quantify dissolved organic nitrogen (DON) or dissolved organic sulfur (DOS) before extraction, but we were able to quantify DOS in SPE-YDOM. While DOS concentrations were $3.56 \pm 0.03 \mu\text{g L}^{-1}$ in Elk Spring SPE-YDOM but only $0.56 \pm 0.01 \mu\text{g L}^{-1}$ in

Octopus Spring SPE-YDOM, SPE-DOC:SPE-DOS molar ratios were lower for Octopus Spring (54 ± 2) than for Elk Spring (108 ± 2). Thus, when compared to DOC, DOS was comparatively larger in SPE-YDOM collected at Octopus Spring.

A theoretical network analysis assuming a simple addition or subtraction of H_2S to DOM molecules (in analogy to a Michael addition reaction) (Heitmann and Blodau, 2006; Tziotis et al., 2011) showed the high diversity of SPE-YDOM sampled from Elk and Octopus Springs (**Figure 9**). Both springs showed CHOS signatures that can be related to CHO signatures, but the diversity at Octopus was limited when compared to Elk Spring. At Octopus, CHOS may be explained by the reactivity of H_2S with DOM because Octopus Spring had measurable quantities of H_2S , but Elk Spring did not (**Table 2**). The origin of the CHOS

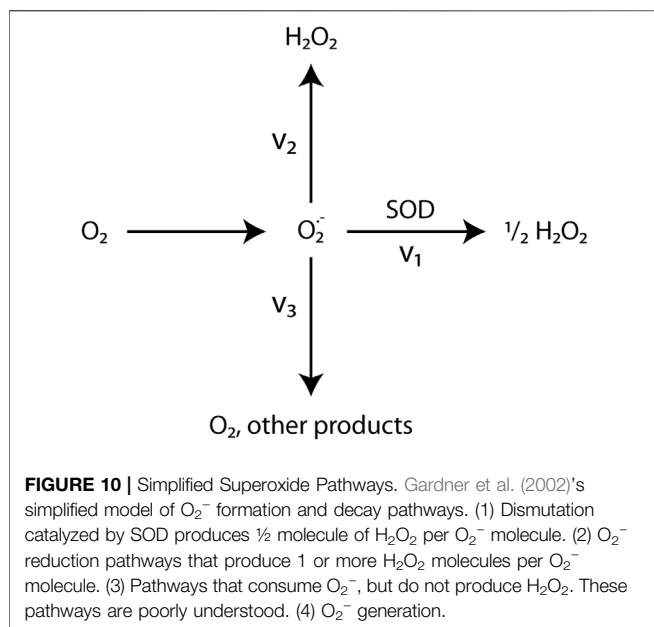


pool at Elk Spring remains unknown because Elk Spring had measurable sulfate and no measurable H₂S. However, perhaps CHO ions can be explained by the loss of H₂S from CHOS precursors, which was highlighted by the results of the network analysis (Figure 9).

4 DISCUSSION

Field and laboratory experiments demonstrated a complex relationship between water composition, Fe speciation, and DOM composition in production and decay of H₂O₂. H₂O₂ concentrations measured in Elk Spring were comparable to those measured in other silica-rich geothermal surface waters in Yellowstone National Park, WY (Wilson et al., 2000a,b; Mesle et al., 2017). This result is not surprising because for the most part, the parent rock for silica-rich hot springs throughout

Yellowstone National Park is silica-rich rhyolite or tuff (e.g., Christiansen, 2001). In our studies, H₂O₂ concentrations corresponded to UV flux, confirming that ROS were primarily formed by photochemical reactions in this system, as previous work suggests (Wilson et al., 2000a). In most systems, ROS are formed by photoreactions with CDOM. However, previous studies by Wilson et al. (2000a) showed that hydrothermal systems have low and variable DOC concentrations throughout the day that do not correspond with H₂O₂ concentrations. Instead, Fe cycling followed a diel pattern that corresponded with H₂O₂ concentrations with increasing Fe²⁺/Fe_{Total} during the day. So, Wilson et al., (2000a) proposed that metal redox reactions are responsible for the majority of ROS formation in high temperature, metal-rich systems. If this is true, H₂O₂ formation should increase with Fe concentration, solubility, and photochemical reactivity. This study confirmed that H₂O₂ formation was higher in Fe-bearing waters than in Fe-



poor waters, that the addition of Fe led to higher H_2O_2 concentrations, and that inactivation of Fe through complexation led to lower H_2O_2 concentrations (Supplementary Tables S2.5, S2.9). Fe complexation did not completely eliminate H_2O_2 production, though, indicating that DOM has a role in H_2O_2 cycling. This role is most apparent in Octopus Spring water where addition of Fe did little to increase the rate of H_2O_2 production. These results suggest that the interplay of different pathways is complex and warrants further investigations.

Although Wilson et al. (2000a) documented that DOC concentrations were unrelated to H_2O_2 cycling, they did not take into account DOM composition. Here we determined the molecular composition and optical properties of SPE-DOM samples to more closely evaluate the relationships between DOM, Fe, and H_2O_2 cycling in hot springs. In addition to Fe addition and chelation experiments, this study also demonstrated that catalyzing superoxide dismutation by addition of SOD, which forces a 2:1 stoichiometry between O_2^- and H_2O_2 , led to lower H_2O_2 production rates. These results are in contrast to those in many fresh and marine surface waters that found higher H_2O_2 photoproduction rates with added SOD (Petasne and Zika, 1997; Garg et al., 2011; Powers and Miller 2016). Because H_2O_2 photoproduction rates were higher without added SOD, reactions with reductants like Fe(II) (Eq. 8) are the dominant pathways of superoxide decay. Metal cycling perhaps plays a role in DOM cycling in these springs, through reactions of DOM and hydroxyl radicals. DOM, in general, and DOS, in particular, were different in Octopus Spring from Elk Spring. DOM had a greater role in Octopus Spring experiments than in Elk Spring experiments likely as a consequence of the differences in water composition.

4.1 Effects of Heat, Cloud Cover, and Wind

Recent reports of the effects of heating on H_2O_2 formation in solutions of up to ~0.5 ionic strength (Bruskov et al., 2002a; b)

raise the question of whether heating in these hot spring systems could also be responsible for H_2O_2 formation (Supplementary Table S2.10). Wilson et al. (2000b) tested this hypothesis in heating experiments (48°C in Fe-rich waters). They found no statistical difference for hot spring waters but found that heating reduced H_2O_2 concentrations in autoclaved, Milli-Q water, which had elevated H_2O_2 concentrations relative to experimental waters at the start of the experiments probably as a result of the autoclave process (Cooper and Zepp, 1990). Elevated temperatures in hot springs probably led to some H_2O_2 production, but, because nighttime concentrations are consistently ~20 nM in our study, the decay term must be of an equal magnitude. In sunlight, however, the photochemical production term exceeds the decay term leading to the elevated concentrations observed here and by Wilson et al. (2000a).

Cloud cover and wind affected surface H_2O_2 production over daily scales (Supplementary Table S2.7). Specifically, July 17 had lower than expected H_2O_2 concentrations given the UV flux. Hence, lower concentrations must have been due to weather conditions (Supplementary Table S2.6). Scattered clouds can temporarily decrease local incident UV irradiance, thereby slowing photochemical H_2O_2 production rates. The measured UV flux was similar on July 17 and July 18. Hence, the differences in H_2O_2 concentrations must be because of strong winds on July 17 likely amplified vertical mixing of H_2O_2 -rich surface waters with H_2O_2 -poor waters at depth, thus diluting surface H_2O_2 concentrations and possibly increasing H_2O_2 at depths. Cooper et al. (1994) and Cooper and Lean (1989) reached a similar conclusion in their studies of a freshwater lake. Field studies at Elk Spring show that the distribution of H_2O_2 can vary dramatically on diel timescales due to variations in weather and wind patterns. These changes in H_2O_2 distribution likely have implications for early microbial evolution and fossil preservation potential at depths. Specifically, if wind leads to vertical mixing of H_2O_2 -rich surface waters to depth then conditions would become more oxidizing causing microbes to adapt and Fe(II) to form insoluble Fe(III)-oxyhydroxides. So, increasing our understanding of weather patterns on early Earth and Mars should allow us to better predict habitability of these systems.

4.2 Field Experiments

Field experiments did not fully replicate natural conditions, i.e., H_2O_2 concentrations in experiments in bags failed to track concentrations in Elk Spring after a cloudy episode (Table 3). This is likely because H_2O_2 is produced continuously *in situ*, assuming there is a constant source of reduced metal. Geothermal springs replenish reactants through constant vertical mixing and continuous influx of a reduced groundwater source. Reduced Fe^{2+} from the source is then oxidized in relatively oxidizing surface waters, thereby producing H_2O_2 (Eqs. 11, 12). This dark, *in situ* pathway sets the base rate for H_2O_2 production. This base rate reaction occurs irrespective of UV flux when reduced metals and oxidants are present, as noted by Yuan et al. (2017). Base rate production was slow, however, because Fe oxidation by O_2 is slow at low pH. In experiments, reduced Fe^{2+} was not replenished, as waters were isolated from the pool in bags. So, reduced Fe^{2+} available for H_2O_2 formation in experimental waters was limited

to what may be produced by photoreduction, i.e., limited by Fe concentration and UV flux. So, the *in situ* H₂O₂ formation base rate was hindered. In other words, *in situ* measurements were likely higher and responded more quickly to variations in UV flux compared to simultaneous field experiments because Fe²⁺ in the field experiments was not replenished, whereas it was replenished in the spring. Additional field studies are necessary to unravel these complex findings and to test whether experimental findings hold true in natural conditions.

4.3 Laboratory Experiments

4.3.1 Effects of Fe Speciation on H₂O₂ Production Rates

The increase in photochemical H₂O₂ formation rates when Fe(III) was added to experiments (Figure 5; Table 4) is a consequence of Fe(III) speciation and solubility (Table 5), which, in turn, are a function of pH due to hydrolysis of the Fe³⁺ ion (Supplementary Table S2.7; Table 5; Parkhurst and Appelo, 1999). In acidic Elk Spring, the first hydrolysis product (Fe(OH)²⁺) and less so, the second hydrolysis product (Fe(OH)₂⁺) dominate the system while in alkaline Octopus Spring, the neutral species (Fe(OH)₃ (aq)) is the dominant species (Supplementary Table S2.11). The first hydrolysis product (Fe(OH)²⁺) is the photochemically active form, and consequently, at higher pH where it is not present as a significant portion of the dissolved Fe(III) species, less H₂O₂ production would be expected. When the strong inorganic chelator, F⁻, was added, fluoride complexes (Table 5) became the dominant species (Supplementary Table S2.11) and H₂O₂ formed more slowly (Table 4). Furthermore, some H₂O₂ production might be attributed to Fe-oxyhydroxide surfaces. Because it binds to surface sites on the iron oxide (Ding et al., 2012), F⁻ effectively reduces the number of photochemically reducible sites and, consequently, could limit the amount of H₂O₂ produced. The effects would be more pronounced in low pH systems where more F⁻ adsorbs to the Fe-oxyhydroxide surface than they would be at higher pH (Ding et al., 2012).

However, some H₂O₂ production occurred in the presence of F⁻ in experiments with both hot spring waters (Figure 5; Table 4). The difference between the production rate with F⁻ and that without F⁻ could represent the production caused by DOM. This difference was approximately the same for Octopus Spring (32%) and Elk Spring (27%) waters suggesting that in each case, some H₂O₂ production occurs via DOM. In these systems, though, photochemical metal redox reactions accounted for more H₂O₂ production than DOM reactions.

4.3.2 Effects of Superoxide Dismutase and Catalase on H₂O₂ Production Rates

This study demonstrated that the removal of superoxide by addition of SOD led to lower H₂O₂ production rates (Figure 5; Table 4). Previous studies found that SOD can increase (Cooper and Zika, 1983; Garg et al., 2007; Powers and Miller, 2016), decrease (Teixeira et al., 1998), or have no effect on H₂O₂ production in irradiated waters (Gardner et al., 2002). The change in H₂O₂ production when SOD is added depends on the ratio between the rates of two O₂^{•-}

TABLE 5 | Speciation and solubility constants for iron species (data from Parkhurst and Appelo, 1999).

Hydrolysis product number	Formation Equation	pK
1	Fe ³⁺ + H ₂ O = Fe(OH) ²⁺ + H ⁺	2.19
2	Fe ³⁺ + 2 H ₂ O = Fe(OH) ₂ ⁺ + 2H ⁺	5.67
3	Fe ³⁺ + 3 H ₂ O = Fe(OH) ₃ + 3H ⁺	12.56
4	Fe ³⁺ + 4 H ₂ O = Fe(OH) ₄ ⁻ + 4H ⁺	21.6
	Fe(OH) ₃ + 3H ⁺ = Fe ³⁺ + 3H ₂ O	-3.96
	Fe ³⁺ + F ⁻ = FeF ²⁺	-6.2
	Fe ³⁺ + 2F ⁻ = FeF ₂ ⁺	-10.8
	Fe ³⁺ + 3F ⁻ = FeF ₃	-14

consuming pathways (Figure 10): those that form one or more molecules of H₂O₂ (v₂) and those that do not form H₂O₂ (v₃) (Petasne and Zika, 1997; Gardner et al., 2002). SOD addition catalyzes dismutation (v₁), shifting O₂^{•-} consumption from v₂ and v₃ to v₁. Dismutation produces ½ H₂O₂ molecule per O₂^{•-} molecule consumed. When pathway v₃ is greater than pathway v₂, SOD addition increases H₂O₂ concentrations because dismutation pathway v₁ produces H₂O₂ while pathway v₃ does not. Conversely, when pathway v₂ is faster than pathway v₃, SOD addition decreases H₂O₂ concentrations because dismutation pathway v₁ produces less H₂O₂ per O₂^{•-} molecule than does pathway v₂ (Gardner et al., 2002). In other words, dismutation competes with a more efficient/higher yield pathway (v₂) (Liochev and Fridovich, 2002), thereby decreasing H₂O₂ yield.

The efficiency of O₂^{•-} conversion in this system to H₂O₂ may decrease as follows: reactions with transition metals are faster than dismutation, which, in turn, is faster than reactions with DOM. Normally, SOD addition drives dismutation and increases H₂O₂ yield in natural water systems (Powers and Miller, 2016). Yet, as noted above, pathway v₂ occurs faster than pathway v₃ in some hydrothermal systems (Gardner et al., 2002). Indeed, known O₂^{•-} reduction pathways include reactions with other ROS (Eq. 5, 18, Figure 1), transition metals (Eq. 8, 18, 19, Figure 1; Wuttig et al., 2013), and/or CDOM (Heller and Croot, 2010a). Consequently, O₂^{•-} decay likely occurs through multiple pathways simultaneously in hot spring systems. However, the dominant O₂^{•-} decay pathway in some hot springs is likely reactions with metals due to high metal and low DOM abundances (Wuttig et al., 2013). Similarly, the dominant O₂^{•-} decay pathway in most natural waters is reactions with DOM because of its relative abundance compared to metals (Heller and Croot, 2010b; Powers and Miller, 2016).

The high reactivity of O₂^{•-} makes it difficult to elucidate the rates and products of various O₂^{•-} decay pathways (Powers et al., 2015; Powers and Miller, 2016). Other factors that may influence SOD's effect on H₂O₂ yield include photochemical efficiency, ionic strength, microbial assemblage, and physiological conditions among others (Petasne and Zika, 1997; Gardner et al., 2002; Powers and Miller, 2016). Of course, there are still many uncertainties surrounding the relationship between O₂^{•-} consumption pathways and H₂O₂ production reactions, especially in natural waters, due to the small number of studies conducted on this topic.

4.3.3 Effects of Particulate Matter

Our work documents no effect of particulate matter on H_2O_2 production in the Fe-bearing, and a positive effect in the Fe-poor, hot springs studied here. In laboratory experiments, the difference in H_2O_2 concentrations between filtered and unfiltered waters is greater for Fe-poor Octopus Spring than it is for Fe-bearing Elk Spring (Table 4). Notably, previous studies have shown that nanophase hematite particles (e.g., Huang et al., 2020) promote photo-production of ROS. So, it is possible that nanophase particles passed through the 0.2- μm filter and contributed to the production of H_2O_2 in Elk Spring experiments with filtered waters. Further work is needed to determine the size distribution and chemical composition of particulate matter to resolve this issue.

Although in the laboratory, Fe-bearing Elk Spring experiments had overall faster formation rates compared to Fe-poor Octopus Spring experiments, particles were more effective at promoting H_2O_2 formation in Octopus Spring water than in Elk Spring water (Table 4, Supplementary Table S2.9). There are two explanations for this: that nanophase Fe-oxyhydroxides are not really removed by filtration for Elk Spring experiments, as mentioned above, or any metals that might be present in Octopus Spring are sequestered to particles, which if present would provide reactive surfaces. The key is whether filtration effectively removes particles or not. In the case of Elk Spring, filtration may not remove the nanophase particles, which then promote production in both filtered and unfiltered experiments, or in the case of Octopus Spring, the particles, which host the metals are, are removed by filtration, leading to lower production in filtered samples. The absence of particle functionality could explain why Octopus Spring water had lower H_2O_2 formation rates than Elk Spring water to begin with.

Field and laboratory experiments yielded contrasting H_2O_2 formation results for Elk Spring experiments depending on whether or not the water was filtered (Table 4). Elk Spring particles had no effect on H_2O_2 production under constant irradiance in the laboratory but decreased H_2O_2 production under variable UV in the field (i.e., formation was faster in bag field experiments when particles were removed, Figure 5 and Tables 3, 4). Rust-colored precipitates around Elk Spring margins contain Fe (Hinman, unpubl.) demonstrating Fe oxidation. So, if Fe(II) present in Elk Spring oxidized on the way to the laboratory, then the resulting Fe(III)-bearing particles could have been removed by sedimentation and filtration prior to laboratory experiments. So, filtration has no effect. On the other hand, we showed that particles promote decay, and so their presence in bag experiments led to lower net formation rates.

Formation rates were marginally higher with particles for Octopus Spring, as well. Because Fe concentrations are below detection in Octopus Spring, the particles themselves may be responsible for increasing UV irradiance because of scattering (Miller and Zepp, 1979). So, light scattering by particles could explain the higher formation rates with particles than without them.

4.4 Effects of Organic Composition

DOC extraction efficiencies were low at both sites (25% at Elk Spring, 4% at Octopus Spring) when compared to oxygenated marine and freshwater samples (Dittmar et al., 2008). DOC extraction efficiencies also decreased with increasing inputs of hydrothermal vent fluids in a previous study (Hawkes et al., 2015), highlighting that the thermal transformation of DOM in hot springs likely creates small organic molecules that are not retained using our extraction procedure. Nonetheless, analyses of SPE-YDOM composition by FT-ICR MS revealed dramatic differences between these two systems. Unique CHO, CHOS, CHNO, and CHNOS signatures at Elk Spring were more oxygenated and spanned a larger mass range than those at Octopus Spring (Figure 8). After SPE, the EEM spectrum at Elk Spring had higher fluorescence intensities than the EEM spectrum of the filtered water sample before extraction, and the SPE-YDOM more resembled EEM spectra typical of oxygenated freshwater DOM (Figure 7). Thus, there may be significant fluorescence quenching in Elk, possibly due to high iron concentrations (Poulin et al., 2014). Previous YDOM characterization at Elk revealed an even distribution of electron-withdrawing (e.g., COOH), neutral, and electron-donating (e.g., OH) aromatic NMR resonances (Gonsior et al., 2018). Electron donating and accepting groups within DOM may contribute to fluorescence properties (Sharpless and Blough, 2014), so these aromatic signatures may contribute to the observed fluorescence signals in Elk Spring SPE-YDOM that are missed when analyzing the filtered water sample. Because photochemical Fe(II) cycling at Elk Spring likely generates abundant hydroxyl radicals (Eqs. 1, 2), perhaps the observed composition reflects hydroxylation of the DOM pool at this site.

SPE-DOS concentrations were significantly higher in Elk Spring SPE-YDOM samples, however, SPE-DOC:SPE-DOS concentrations were larger at Elk (C:S = 108) when compared to Octopus Spring (C:S = 54). While there was less DOS when normalized to DOC at Elk Spring, the CHOS pool was more diverse. Because Elk Spring is an acidic spring with relatively high sulfate concentrations (Table 2), one explanation for the diversity of the CHOS pool is due to the formation of organosulfates via sulfate radical reactions or sulfate anion reactions. The formation of organosulfates in secondary organic aerosols (SOAs) has been well documented (Darer et al., 2011; Kristensen and Glasius, 2011; Schindelka et al., 2013; Chen et al., 2020; Ren et al., 2021) and hydroxyl radical reactions can generate highly oxidized organosulfates (Chen et al., 2020), and hydroxyl radicals are expected to be abundant in this system (Eq. 9). In fact, the abundance of CHOS ions in SOAs increased with increasing SO_2 , sulfate, and photochemical activity (Schmitt-Kopplin et al., 2010). In this study, sulfonation, or the incorporation of sulfur and oxygen (SO_3) into the CHOS pool, was evident. In particular, the formation of sulfate esters from oxidized terpenes was observed (Schmitt-Kopplin et al., 2010), which may be consistent with the highly oxidized CHOS pool observed at Elk Spring.

While DOC extraction efficiencies were very low at Octopus Spring, unique SPE-YDOM had a very different composition at

this site with generally low O/C ratios around ~0.3 and low mass <400 Da. Intriguingly, while SPE-DOC concentrations were much lower at Octopus Spring, SPE-YDOM absorbance spectra were very similar between the two sites when normalized to SPE-DOC concentration. Typically, absorbance features like $a(\lambda)/[\text{DOC}]$ ($\text{L mg}^{-1} \text{ m}^{-1}$) values at 254 nm and absorbance ratios (e.g., $A(250 \text{ nm})/A(365 \text{ nm})$) or spectral slopes have been used as indicators of DOM aromaticity (Weishaar et al., 2003) and molecular weight (Helms et al., 2008). Given the extreme differences in composition and chemistries between these two springs, simple optical indicators of DOM composition are not appropriate in these systems, especially since optical properties can change dramatically depending on sample matrix (e.g., pH, cations, anions, etc). Despite the similarities in absorbance spectra, the EEM spectrum for Octopus Spring SPE-YDOM had unique features not typical of terrestrial or marine systems (Figure 7). Previous work has noted low fluorescence signals and DOC concentrations in alkaline Yellowstone springs and has suggested that tyrosine-like fluorescence (i.e., ex/em ~ 270 nm/310 nm) predominates in these systems (Nye et al., 2020). While there was a large fluorescence signal in this region in the filtered Octopus sample before SPE, this feature was not retained post-SPE (Figure 6). Rather, SPE-YDOM at Octopus Spring could represent fluorescence signatures unique to hydrothermal inputs, and possibly organo-sulfur fluorophores (Nye et al., 2020). Furthermore, fluorescence intensities were higher at Octopus Spring in the excitation/emission (ex/em) regions ranging from 240 to 320 nm/310–500 nm, suggesting there is also something at Octopus Spring that quenches fluorescence in filtered water. Perhaps this observation explains why the scopoletin method did not work *in situ* at this site.

A large fraction of the CHOS pool at Octopus Spring could be explained by sulfurization reactions (H_2S addition). This suggests that the DOS pool is largely reduced when compared to Elk Spring. Recent work has suggested DOS can be preferentially photodegraded relative to bulk DOM in sulfidic porewaters (Gomez-Saez et al., 2017). A subsequent study tested various natural DOM sources and found that DOS is very photolabile when exposed to solar radiation, with the highest degradation rates from sources with reduced DOS (i.e., porewaters) (Ossola et al., 2019). While H_2S was not measured in Octopus Spring during this study, the sulfate measured at this site could be due to photochemical production from the DOS pool. Regardless, because Fe(II) and H_2O_2 could not be detected at Octopus Spring *in situ*, hydroxyl radical reactions are likely minimal at this site.

4.5 Decay Experiments

In our laboratory studies, water chemistries that yielded the fastest photochemical H_2O_2 formation also yielded the fastest decay rates (Figure 5). Our decay experiments confirmed that particulate matter has a primary role and soluble matter has a secondary role in H_2O_2 decay; particulate matter roughly doubled the decay rate in both Elk Spring and Octopus Spring waters. Indeed, both soluble and insoluble species

promoted H_2O_2 degradation compared to MilliQ rates. H_2O_2 decay rates were faster in Elk Spring water than in Octopus Spring water, even when Fe^{3+} was added to the latter indicating the importance of dissolved Fe species in decay; the effect is greater for the decay mechanism than for the formation mechanism. Similarly, deionized water had the slowest H_2O_2 decay rates because it lacks both particulate and soluble matter. Consequently, unfiltered Elk Spring water yielded the fastest H_2O_2 degradation rates. Rates of other water types varied between these two end members due to the opposing roles of particulate and soluble matter in decay.

This result contradicts Wilson et al. (2000b) study, which found no statistical decrease in H_2O_2 concentrations after 24 h in experiments with filtered water, indicating that dissolved matter was unimportant in ROS decay. Wilson et al. (2000b) studied a hot spring with different water chemistry, and this discrepancy can likely be explained by higher concentrations of Fe coupled with higher pH (0.10 mM, pH 5.6, Wilson et al., 2000a) compared to Elk Spring (0.01 mM, pH 3.3–4.2). It is likely that Fe solids formed in their water samples before filtration and, therefore, dissolved matter was removed along with particulate matter upon filtration. Consequently, filtered waters experienced little to no H_2O_2 decay in Wilson et al.'s (2000b) experiments in contrast to the results reported here.

4.6 Dark H_2O_2 Production and Decay

The H_2O_2 formed in filtered, Fe-bearing Elk Spring and Fe-added experiments in the dark most likely proceeds differently than the undefined biological mechanisms proposed in DOM-rich systems (Dixon et al., 2013; Marsico et al., 2015). Indeed, it is unlikely that dark H_2O_2 production mechanisms were biologic as both waters were sterile filtered and because deionized and Elk Spring water (Wilson et al., 2000a; Gonsior et al., 2018) presumably had low organic contents to begin with. Yuan et al. (2017) found that light-independent H_2O_2 formation can occur through a previously unrecognized pathway that involves the oxidation of reduced elements, like metals and natural organic matter, by oxygen at redox interfaces. So, while it is possible that biologic mechanisms were involved in dark formation in this study because experiments were not run in a completely sterile environment (discussed in methods section), the pathways proposed by Yuan et al. (2017) were most likely responsible for dark H_2O_2 production here. Further investigation is still necessary, however, to determine the importance and pathways of dark H_2O_2 production in these systems. Understanding dark H_2O_2 reactions may explain anomalous H_2O_2 concentrations in metal-rich waters.

4.7 Implications for Mars

The pathways to ROS production on Mars confront us with an interesting paradox. The time from 4.3 to 3.8 Ga was, in general, more favorable to the development of life as we know it and the production of organic matter. However, the combination of the Heavy Bombardment with peak

hydrogeological activity and erosion made it also the most destructive period, and destructive physical and mechanical processes could have limited biosignature preservation. After 3.8 Ga, environmental conditions were, by contrast, somewhat more favorable to ROS formation, i.e., increased UV and ionizing radiation, but it was also a time when conditions became hostile at the surface for life. Therefore, even though conditions were favorable then for preservation, there was likely no biological record left to preserve at the surface.

If life had sought refuge underground (or was always) underground, biosignatures could have been preserved in localized refuges. Indeed, volcanism continued after 3.8 Ga. For example, the Tharsis volcanoes continued to grow after 3.8 Ga, and Elysium started its build up around 3.4 Ga. The geological record of that time shows residual hydrological activity at the surface and in the subsurface, which supports the hypothesis that hydrothermal activity could still have been common during the Hesperian. Further, recent volcanoes (200,000–500,000 years) have been identified in Valles Marineris (Broz et al., 2017) and fissural activity (~50,000 years old) in the Cerberus area East of Elysium Planitia (Horvath et al., 2021). As ice and water persist in the subsurface even now (Lauro et al., 2021) and because crustal water (subsurface water and ice along with structural water in minerals) could account for up to 94% of water lost during the Noachian period (Scheller et al., 2021), the potential remains for hydrothermal activity at present (Cady et al., 2018), and hot springs would be candidates for ROS-induced biosignature preservation.

While the composition of Mars's early atmosphere remains unclear, recent findings of Mn-oxides suggest that Mars's atmospheric evolution was complex, and O_2 -levels may have been higher compared to present day concentrations, although still relatively low (Lanza et al., 2016). O_2 , therefore, may have had more of a role in ROS production on early Mars than previously thought. However, ROS concentrations produced by reactions not requiring O_2 were more likely higher at that time. ROS could have been important primary oxidants and, therefore, the most likely to oxidize Fe^{2+} to Fe^{3+} , which then could preserve biosignatures. Hot springs on Mars could have had significant Fe concentrations. Coupled with our findings that ROS formation in Fe-rich hot springs is largely controlled by photochemical Fe redox reactions, such conditions on Mars would have a high biosignature preservation potential.

5 CONCLUSION

Our work showed that, Fe-bearing geothermal water yielded faster photochemical H_2O_2 formation and dark decay rates than Fe-poor water. H_2O_2 concentrations were largely controlled by the presence and speciation of Fe, i.e. whether Fe was present in a photochemically active state or not. Particulate matter appeared to have little effect on formation in ACIS Fe-bearing Elk Spring but did in AlkCl Fe-poor Octopus Spring. However, the possibility cannot be ruled out that nanophase particles were largely responsible for H_2O_2

production in Elk Spring. Particulate matter had a primary role in H_2O_2 decay. Consequently, this study highlights the effects of both insoluble and soluble Fe species on the rate of H_2O_2 cycling. In the absence of Fe, DOM dominated H_2O_2 cycling.

The various pathways for ROS production in hot springs are only just being elucidated, and early work shows that they are complicated by interacting metal and DOM reactions. The pathways under oxic conditions (Eq. 7) produce $O_2^{\cdot-}$ (Eqs. 2, 7). Therefore, $O_2^{\cdot-}$ concentrations should be limited along with O_2 , as would be expected to prevail on early Mars. Our results suggest that in the presence of iron and, for the most part, H_2O_2 production is not limited by and so could be quickly produced in anoxic or low oxygen conditions by the photohydrolysis of dissolved Fe(III) or Fe (or other)-oxyhydroxides (Eq. 9). H_2O_2 concentrations in low O_2 or anoxic waters on Mars may have reached higher H_2O_2 concentrations than those measured in modern analogs because of the lack of competing $O_2^{\cdot-}$ pathways. So, assuming life on Mars, rapid Fe^{2+} oxidation by photochemically produced ROS was possible. Warren and Ferris (1998) demonstrated that bacterial cell surfaces take up Fe(III) in the form of hydrous ferric oxide. Rapid entombment by Fe-oxides has the potential to preserve biosignatures in the earliest stages of diagenesis. Indeed, Fe^{3+} can bind to negatively charged cell membranes and promote lipid preservation (Parenteau et al., 2014). Monomeric Si can coprecipitate with these Fe cations to isolate and potentially preserve morphological biosignatures in the rock record (Parenteau and Cady, 2010). Hence, it is possible that this mechanism enabled organic molecules to enter the rock record on early Mars. By understanding the coupling of the biogeochemical cycles of Fe with the cycles of ROS, we are better equipped to pinpoint geochemical and mineralogical signatures in potentially habitable environments on Mars that could be tied to living systems as biosignatures.

DATA AVAILABILITY STATEMENT

The original contributions presented in the study are included in the article/**Supplementary Material**, further inquiries can be directed to the corresponding author.

AUTHOR CONTRIBUTIONS

MM and NH designed all experiments. MM performed all analyses and experiments. MG and LP performed DOM and DOS analyses. All authors interpreted the results and wrote the manuscript.

FUNDING

The authors acknowledge support from NASA Astrobiology Institute (Grant Nos. NNX15BB01A, NC, PI, SETI Institute)

and Sigma Xi Grant-in-Aid of Research. Funded by the Deutsche Forschungsgemeinschaft (DFG, German Research Foundation) - Project ID 364653263 TRR 235 (CRC 235).

ACKNOWLEDGMENTS

The authors appreciate analytical support from the University of Montana's Biogeochemistry Lab and SGS Canada. The authors

thank the Yellowstone Center for Resources for permitting this work within the Park (Permit # YELL-2017-SCI-1660). Comments from reviewers greatly improved the manuscript.

SUPPLEMENTARY MATERIAL

The Supplementary Material for this article can be found online at: <https://www.frontiersin.org/articles/10.3389/fspas.2022.727015/full#supplementary-material>

REFERENCES

- Alleon, J., Bernard, S., Le Guillou, C., Daval, D., Skouri-Panet, F., Pont, S., et al. (2016). Early Entombment within Silica Minimizes the Molecular Degradation of Microorganisms during Advanced Diagenesis. *Chem. Geol.* 437, 98–108. doi:10.1016/j.chemgeo.2016.05.034
- Ball, J. W., Mcmleskey, R. B., and Nordstrom, D. K. (2010). "Water-chemistry Data for Selected Springs, Geysers, and Streams in Yellowstone National Park, Wyoming, 2006-2008," in *Open-File Report* (Reston, VA C6).
- Baratoux, D., Toplis, M. J., Monnereau, M., and Gasnault, O. (2011). Thermal History of Mars Inferred from Orbital Geochemistry of Volcanic Provinces. *Nature* 472, 338–341. doi:10.1038/nature09903
- Benkelberg, H.-J., and Warneck, P. (1995). Photodecomposition of Iron(III) Hydroxo and Sulfato Complexes in Aqueous Solution: Wavelength Dependence of OH and SO₄⁻ Quantum Yields. *J. Phys. Chem.* 99, 5214–5221. doi:10.1021/j100014a049
- Bianco, A., Passananti, M., Brigante, M., and Mailhot, G. (2020). Photochemistry of the Cloud Aqueous Phase: A Review. *Molecules* 25. doi:10.3390/molecules25020423
- Bielski, B. H. J., Cabelli, D. E., Arudi, R. L., and Ross, A. B. (1985). Reactivity of HO₂/O₂⁻ Radicals in Aqueous Solution. *J. Phys. Chem. Reference Data* 14, 1041–1100. doi:10.1063/1.555739
- Blough, N. V., and Del Vecchio, R. (2018). Comment on the Case against Charge Transfer Interactions in Dissolved Organic Matter Photophysics. *Environ. Sci. Technol.* 52, 5512–5513. doi:10.1021/acs.est.8b01189
- Blough, N. V., and Zepp, R. G. (1995). "Reactive Oxygen Species in Natural Waters," in *Active Oxygen in Chemistry* (Springer), 280–333. doi:10.1007/978-94-007-0874-7_8
- Bottke, W. F., Vokrouhlický, D., Minton, D., Nesvorný, D., Morbidelli, A., Brasser, R., et al. (2012). An Archaean Heavy Bombardment from a Destabilized Extension of the Asteroid Belt. *Nature* 485 (7396), 78–81. doi:10.1038/nature10967
- Brioukhanov, A. L., Netrusov, A. I., and Eggen, R. I. L. (2006). The Catalase and Superoxide Dismutase Genes Are Transcriptionally Up-Regulated upon Oxidative Stress in the Strictly Anaerobic Archaeon Methanosarcina Barkeri. *Microbiology-Sgm* 152, 1671–1677. doi:10.1099/mic.0.28542-0
- Brož, P., Hauber, E., Wray, J. J., and Michael, G. (2017). Amazonian Volcanism inside Valles Marineris on Mars. *Earth Planet. Sci. Lett.* 473, 122–130.
- Bruskov, V. I., Malakhova, L. V., Masalimov, Z. K., and Chernikov, A. V. (2002a). Heat-induced Formation of Reactive Oxygen Species and 8-oxoguanine, a Biomarker of Damage to DNA. *Nucleic Acids Res.* 30, 1354–1363. doi:10.1093/nar/30.6.1354
- Bruskov, V. I., Masalimov, Z. K., and Chernikov, A. V. (2002b). Heat-induced Generation of Reactive Oxygen Species in Water. *Doklady. Biochem. biophys* 384, 181–184. doi:10.1023/a:1016036617585
- Butturini, A., Amalfitano, S., Herzsprung, P., Lechtenfeld, O., Venturi, S., Olaka, L. A., et al. (2020). Dissolved Organic Matter in Continental Hydro-Geothermal Systems: Insights from Two Hot Springs of the East African Rift Valley. *USDA* 12. doi:10.3390/w12123512
- Cabrol, N. A. (2018). The Coevolution of Life and Environment on Mars: An Ecosystem Perspective on the Robotic Exploration of Biosignatures. *Astrobiology* 18, 1–27. doi:10.1089/ast.2017.1756
- Cady, S. L., and Farmer, J. D. (1996). Fossilization Processes in Siliceous Thermal Springs: Trends in Preservation along Thermal Gradients. *Ciba Found. Symp.* 202, 150–153. doi:10.1002/9780470514986.ch9
- Cady, S. L., Farmer, J. D., Grotzinger, J. P., Schopf, J. W., and Steele, A. (2003). Morphological Biosignatures and the Search for Life on Mars. *Astrobiology* 3, 351–368. doi:10.1089/153110703769016442
- Cady, S. L., Skok, J. R., Gulick, V. G., Berger, J. A., and Hinman, N. W. (2018). "Siliceous Hot Spring Deposits: Why They Remain Key Astrobiological Targets," in *From Habitability to Life on Mars*. Editors N. Cabrol, E. G. Cabrol, and N. Grin (Edmond: Elsevier), 179–210. doi:10.1016/b978-0-12-809935-3.00007-4
- Campbell, K. A., Guido, D. M., Gautret, P., Foucher, F., Ramboz, C., and Westall, F. (2015). Geysereite in Hot-Spring Siliceous Sinter: Window on Earth's Hottest Terrestrial (Paleo)environment and its Extreme Life. *Earth-Science Rev.* 148, 44–64. doi:10.1016/j.earscirev.2015.05.009
- Chen, J., and Browne, W. R. (2018). Photochemistry of Iron Complexes. *Coord. Chem. Rev.* 374, 15–35. doi:10.1016/j.ccr.2018.06.008
- Chen, Y., Zhang, Y., Lambe, A. T., Xu, R., Lei, Z., Olson, N. E., et al. (2020). Heterogeneous Hydroxyl Radical Oxidation of Isoprene-Epoxydiol-Derived Methyltetrol Sulfates: Plausible Formation Mechanisms of Previously Unexplained Organosulfates in Ambient Fine Aerosols. *Environ. Sci. Technol. Lett.* 7, 460–468. doi:10.1021/acs.estlett.0c00276
- Christiansen, R. I. (2001). *The Quaternary and Pliocene Yellowstone Plateau Volcanic Field of Wyoming, Idaho, and Montana*. Reston, VA: U.S. Geological Survey.
- Cockell, C. S. (2000). The Ultraviolet History of the Terrestrial Planets - Implications for Biological Evolution. *Planet. Space Sci.* 48, 203–214. doi:10.1016/s0032-0633(99)00087-2
- Cohen, B. A., Swindle, T. D., and Kring, D. A. (2000). Support for the Lunar Cataclysm Hypothesis from Lunar Meteorite Impact Melt Ages. *Science* 290 (5497), 1754–1756. doi:10.1126/science.290.5497.1754
- Cooper, W. J., and Lean, D. R. S. (1989). Hydrogen Peroxide Concentration in a Northern Lake: Photochemical Formation and Diel Variability. *Environ. Sci. Technol.* 23, 1425–1428. doi:10.1021/es00069a017
- Cooper, W. J., Moegling, J. K., Kieber, R. J., and Kiddle, J. J. (2000). A Chemiluminescence Method for the Analysis of H₂O₂ in Natural Waters. *Mar. Chem.* 70, 191–200. doi:10.1016/s0304-4203(00)00025-6
- Cooper, W. J., Shao, C., Lean, D. R., Gordon, A. S., and Scully, F. E., Jr (1994). Factors Affecting the Distribution of H₂O₂ in Surface Waters. *Adv. Chem.* 237, 391–422. doi:10.1021/ba-1994-0237.ch012
- Cooper, W. J., and Zepp, R. G. (1990). Hydrogen Peroxide Decay in Waters with Suspended Soils: Evidence for Biologically Mediated Processes. *Can. J. Fish. Aquat. Sci.* 47, 888–893. doi:10.1139/f90-102
- Cooper, W. J., and Zika, R. G. (1983). Photochemical Formation of Hydrogen Peroxide in Surface and Ground Waters Exposed to Sunlight. *Science* 220, 711–712. doi:10.1126/science.220.4598.711
- Damer, B., and Deamer, D. (2015). Coupled Phases and Combinatorial Selection in Fluctuating Hydrothermal Pools: A Scenario to Guide Experimental Approaches to the Origin of Cellular Life. *Life* 5, 872–887. doi:10.3390/life5010872
- Darar, A. I., Cole-Filipiak, N. C., O'Connor, A. E., and Elrod, M. J. (2011). Formation and Stability of Atmospherically Relevant Isoprene-Derived Organosulfates and Organonitrates. *Environ. Sci. Technol.* 45, 1895–1902. doi:10.1021/es103797z

- De Wet, C. B., and Davis, K. (2010). Preservation Potential of Microorganism Morphologies in Tufas, Sinters, and Travertines through Geologic Time. *Palaeobio Palaeoenviron* 90, 139–152. doi:10.1007/s12549-010-0027-z
- Des Marais, D. J., and Walter, M. R. (2019). Terrestrial Hot Spring Systems: Introduction. *Astrobiology* 19, 1419–1432. doi:10.1089/ast.2018.1976
- Ding, X., Song, X., and Boily, J.-F. (2012). Identification of Fluoride and Phosphate Binding Sites at FeOOH Surfaces. *J. Phys. Chem. C* 116, 21939–21947. doi:10.1021/jp3083776
- Dittmar, T., Koch, B., Hertkorn, N., and Kattner, G. (2008). A Simple and Efficient Method for the Solid-phase Extraction of Dissolved Organic Matter (SPEDOM) from Seawater. *Limnol. Oceanogr. Methods* 6, 230–235. doi:10.4319/lom.2008.6.230
- Dixon, T. C., Vermilyea, A. W., Scott, D. T., and Voelker, B. M. (2013). Hydrogen Peroxide Dynamics in an Agricultural Headwater Stream: Evidence for Significant Nonphotochemical Production. *Limnol. Oceanogr.* 58, 2133–2144. doi:10.4319/lo.2013.58.6.2133
- Farmer, J. D., and Des Marais, D. J. (1999). Exploring for a Record of Ancient Martian Life. *J. Geophys. Res.* 104, 26977–26995. doi:10.1029/1998je000540
- Faust, B. C., and Allen, J. M. (1993). Aqueous-phase Photochemical Formation of Hydroxyl Radical in Authentic Cloudwaters and Fogwaters. *Environ. Sci. Technol.* 27, 1221–1224. doi:10.1021/es00043a024
- Fernández-Remolar, D. C., Prieto-Ballesteros, O., Rodríguez, N., Gómez, F., Amils, R., Gómez-Elvira, J., et al. (2008). Underground Habitats in the Río Tinto Basin: A Model for Subsurface Life Habitats on Mars. *Astrobiology* 8, 1023–1047. doi:10.1089/ast.2006.0104
- Fournier, R. O. (1989). Geochemistry and Dynamics of the Yellowstone National Park Hydrothermal System. *Annu. Rev. Earth Planet. Sci.* 17, 13–53. doi:10.1146/annurev.ea.17.050189.000305
- Gao, H., and Zepp, R. G. (1998). Factors Influencing Photoreactions of Dissolved Organic Matter in a Coastal River of the Southeastern United States. *Environ. Sci. Technol.* 32, 2940–2946. doi:10.1021/es9803660
- Gardner, R., Salvador, A., and Moradas-Ferreira, P. (2002). Why Does SOD Overexpression Sometimes Enhance, Sometimes Decrease, Hydrogen Peroxide Production? A Minimalist Explanation. *Free Radic. Biol. Med.* 32, 1351–1357. doi:10.1016/s0891-5849(02)00861-4
- Gardner, W. P., Susong, D. D., Solomon, D. K., and Heasler, H. P. (2011). A Multitracer Approach for Characterizing Interactions between Shallow Groundwater and the Hydrothermal System in the Norris Geyser Basin Area, Yellowstone National Park. *Geochem. Geophys. Geosystems* 12. doi:10.1029/2010gc003353
- Garg, S., Rose, A. L., and Waite, T. D. (2011). Photochemical Production of Superoxide and Hydrogen Peroxide from Natural Organic Matter. *Geochimica Cosmochimica Acta* 75, 4310–4320. doi:10.1016/j.gca.2011.05.014
- Garg, S., Rose, A. L., and Waite, T. D. (2007). Production of Reactive Oxygen Species on Photolysis of Dilute Aqueous Quinone Solutions. *Photochem. Photobiol.* 83, 904–913. doi:10.1111/j.1751-1097.2007.00075.x
- Gomez-Saez, G. V., Pohlbeln, A. M., Stubbins, A., Marsay, C. M., and Dittmar, T. (2017). Photochemical Alteration of Dissolved Organic Sulfur from Sulfidic Porewater. *Environ. Sci. Technol.* 51, 14144–14154. doi:10.1021/acs.est.7b03713
- Gonsior, M., Hertkorn, N., Hinman, N., Dvorski, S. E., Harir, M., Cooper, W. J., et al. (2018). Yellowstone Hot Springs Are Organic Chemodiversity Hot Spots. *Sci. Rep.* 8, 14155. doi:10.1038/s41598-018-32593-x
- Gonsior, M., Peake, B. M., Cooper, W. T., Podgorski, D. C., D'andrilli, J., Dittmar, T., et al. (2011). Characterization of Dissolved Organic Matter across the Subtropical Convergence off the South Island, New Zealand. *Mar. Chem.* 123, 99–110. doi:10.1016/j.marchem.2010.10.004
- Gonsior, M., Peake, B. M., Cooper, W. T., Podgorski, D., D'andrilli, J., and Cooper, W. J. (2009). Photochemically Induced Changes in Dissolved Organic Matter Identified by Ultrahigh Resolution Fourier Transform Ion Cyclotron Resonance Mass Spectrometry. *Environ. Sci. Technol.* 43, 698–703. doi:10.1021/es8022804
- Gonsior, M., Schmitt-Kopplin, P., and Bastviken, D. (2013). Depth-dependent Molecular Composition and Photo-Reactivity of Dissolved Organic Matter in a Boreal Lake under Winter and Summer Conditions. *Biogeosciences* 10, 6945–6956. doi:10.5194/bg-10-6945-2013
- Gonsior, M., Schmitt-Kopplin, P., Stavklint, H., Richardson, S. D., Hertkorn, N., and Bastviken, D. (2014). Changes in Dissolved Organic Matter during the Treatment Processes of a Drinking Water Plant in Sweden and Formation of Previously Unknown Disinfection Byproducts. *Environ. Sci. Technol.* 48, 12714–12722. doi:10.1021/es504349p
- Guidry, S. A., and Chafetz, H. S. (2003). Anatomy of Siliceous Hot Springs: Examples from Yellowstone National Park, Wyoming, USA. *Sediment. Geol.* 157, 71–106. doi:10.1016/s0037-0738(02)00195-1
- Hawkes, J. A., Rossel, P. E., Stubbins, A., Butterfield, D., Connelly, D. P., Achterberg, E. P., et al. (2015). Efficient Removal of Recalcitrant Deep-Ocean Dissolved Organic Matter during Hydrothermal Circulation. *Nat. Geosci.* 8, 856–860. doi:10.1038/ngeo2543
- He, S., Chen, Z., Zhang, X., Zhao, Y., Huang, D., Zhao, J., et al. (2010). Measurement of Atmospheric Hydrogen Peroxide and Organic Peroxides in Beijing before and during the 2008 Olympic Games: Chemical and Physical Factors Influencing Their Concentrations. *J. Geophys. Res. Atmos.* 115. doi:10.1029/2009jd013544
- Heitmann, T., and Blodau, C. (2006). Oxidation and Incorporation of Hydrogen Sulfide by Dissolved Organic Matter. *Chem. Geol.* 235, 12–20. doi:10.1016/j.chemgeo.2006.05.011
- Heller, M. I., and Croot, P. L. (2010a). Kinetics of Superoxide Reactions with Dissolved Organic Matter in Tropical Atlantic Surface Waters Near Cape Verde (TENATSO). *J. Geophys. Res.* 115, C12038. doi:10.1029/2009jc006021
- Heller, M. I., and Croot, P. L. (2010b). Superoxide Decay Kinetics in the Southern Ocean. *Environ. Sci. Technol.* 44, 191–196. doi:10.1021/es901766r
- Helms, J. R., Stubbins, A., Ritchie, J. D., Minor, E. C., Kieber, D. J., and Mopper, K. (2008). Absorption Spectral Slopes and Slope Ratios as Indicators of Molecular Weight, Source, and Photobleaching of Chromophoric Dissolved Organic Matter. *Limnol. Oceanogr.* 53, 955–969. doi:10.4319/lo.2008.53.3.0955
- Hertkorn, N., Ruecker, C., Meringer, M., Gugisch, R., Frommberger, M., Perdue, E. M., et al. (2007). High-precision Frequency Measurements: Indispensable Tools at the Core of the Molecular-Level Analysis of Complex Systems. *Anal. Bioanal. Chem.* 389, 1311–1327. doi:10.1007/s00216-007-1577-4
- Hertzog, J., Naraoka, H., and Schmitt-Kopplin, P. (2019). Profiling Murchison Soluble Organic Matter for New Organic Compounds with APPI- and ESI-FT-ICR MS. *Life (Basel)* 9. doi:10.3390/life9020048
- Herzprung, P., Osterloh, K., von Tümpling, W., Harir, M., Hertkorn, N., Schmitt-Kopplin, P., et al. (2017). Differences in DOM of Rewetted and Natural Peatlands - Results from High-Field FT-ICR-MS and Bulk Optical Parameters. *Sci. Total Environ.* 586, 770–781. doi:10.1016/j.scitotenv.2017.02.054
- Holm, T. R., George, G. K., and Barcelona, M. J. (1987). Fluorometric Determination of Hydrogen Peroxide in Groundwater. *Anal. Chem.* 59, 582–586. doi:10.1021/ac00131a010
- Horvath, D. G., Moitra, P., Hamilton, C. W., Craddock, R. A., and Andrews-Hanna, J. C. (2021). Evidence for Geologically Recent Explosive Volcanism in Elysium Planitia, Mars. *Icarus* 365, 114499. doi:10.1016/j.icarus.2021.114499
- Huang, X., Zhao, Q., Young, R. P., Zhang, X., Walter, E. D., Chen, Y., et al. (2020). Photo-production of Reactive Oxygen Species and Degradation of Dissolved Organic Matter by Hematite Nanoplates Functionalized by Adsorbed Oxalate. *Environ. Sci. Nano* 7, 2278–2292. doi:10.1039/d0en00365d
- Hurwitz, S., and Lowenstern, J. B. (2014). Dynamics of the Yellowstone Hydrothermal System. *Rev. Geophys.* 52, 375–411. doi:10.1002/2014rg000452
- Johnson, K. S., Coale, K. H., Elrod, V. A., and Tindale, N. W. (1994). Iron Photochemistry in Seawater from the Equatorial Pacific. *Mar. Chem.* 46, 319–334. doi:10.1016/0304-4203(94)90029-9
- Jones, B., Renaut, R. W., and Rosen, M. R. (2001). Microbial Construction of Siliceous Stalactites at Geysers and Hot Springs: Examples from the Whakarewarewa Geothermal Area, North Island, New Zealand. *Palaios* 16, 73–94. doi:10.1669/0883-1351(2001)016<0073:mccosa>2.0.co;2
- Jones, B., and Renaut, R. W. (2007). Selective Mineralization of Microbes in Fe-Rich Precipitates (Jarosite, Hydrated Ferric Oxides) from Acid Hot Springs in the Waioatapu Geothermal Area, North Island, New Zealand. *Sediment. Geol.* 194, 77–98. doi:10.1016/j.sedgeo.2006.05.025
- Kellerman, A. M., Guillemette, F., Podgorski, D. C., Aiken, G. R., Butler, K. D., and Spencer, R. G. M. (2018). Unifying Concepts Linking Dissolved Organic Matter Composition to Persistence in Aquatic Ecosystems. *Environ. Sci. Technol.* 52, 2538–2548. doi:10.1021/acs.est.7b05513
- Kieber, D. J., Miller, G. W., Neale, P. J., and Mopper, K. (2014). Wavelength and Temperature-dependent Apparent Quantum Yields for Photochemical

- Formation of Hydrogen Peroxide in Seawater. *Environ. Sci. Process. Impacts* 16, 777–791. doi:10.1039/c4em00036f
- Klein, C. (2005). Some Precambrian Banded Iron-Formations (BIFs) from Around the World: Their Age, Geologic Setting, Mineralogy, Metamorphism, Geochemistry, and Origins. *Am. Mineralogist* 90, 1473–1499. doi:10.2138/am.2005.1871
- Koch, M., Rudolph, C., Moissl, C., and Huber, R. (2006). A Cold-Loving Crenarchaeon Is a Substantial Part of a Novel Microbial Community in Cold Sulphidic Marsh Water. *FEMS Microbiol. Ecol.* 57, 55–66. doi:10.1111/j.1574-6941.2006.00088.x
- Konhauser, K. O., and Ferris, F. G. (1996). Diversity of Iron and Silica Precipitation by Microbial Mats in Hydrothermal Waters, Iceland: Implications for Precambrian Iron Formations. *Geol.* 24, 323–326. doi:10.1130/0091-7613(1996)024<0323:doiasp>2.3.co;2
- Koppenol, W. H. (2001). The Haber-Weiss Cycle - 70 Years Later. *Redox Rep.* 6, 229–234. doi:10.1179/135100001101536373
- Kranendonk, M. J. V. (2018). The Setting for the Origin of Life: a Geological-Geochemical Perspective. *Biochem.* 40, 18–21. doi:10.1042/bio04006018
- Kremer, M. L. (2003). The Fenton Reaction. Dependence of the Rate on pH. *J. Phys. Chem. A* 107, 1734–1741. doi:10.1021/jp020654p
- Kristensen, K., and Glasius, M. (2011). Organosulfates and Oxidation Products from Biogenic Hydrocarbons in Fine Aerosols from a Forest in North West Europe during Spring. *Atmos. Environ.* 45, 4546–4556. doi:10.1016/j.atmosenv.2011.05.063
- Ksionzek, K. B., Lechtenfeld, O. J., Mccallister, S. L., Schmitt-Kopplin, P., Geuer, J. K., Geibert, W., et al. (2016). Dissolved Organic Sulfur in the Ocean: Biogeochemistry of a Petagram Inventory. *Science* 354, 456–459. doi:10.1126/science.aaf7796
- Kujawinski, E. B., Del Vecchio, R., Blough, N. V., Klein, G. C., and Marshall, A. G. (2004). Probing Molecular-Level Transformations of Dissolved Organic Matter: Insights on Photochemical Degradation and Protozoan Modification of DOM from Electrospray Ionization Fourier Transform Ion Cyclotron Resonance Mass Spectrometry. *Mar. Chem.* 92, 23–37. doi:10.1016/j.marchem.2004.06.038
- Kyle, J. E., Schroeder, P. A., and Wiegel, J. (2007). Microbial Silicification in Sinters from Two Terrestrial Hot Springs in the Uzon Caldera, Kamchatka, Russia. *Geomicrobiol. J.* 24, 627–641. doi:10.1080/01490450701672158
- Lanza, N. L., Wiens, R. C., Arvidson, R. E., Clark, B. C., Fischer, W. W., Gellert, R., et al. (2016). Oxidation of Manganese in an Ancient Aquifer, Kimberley Formation, Gale Crater, Mars. *Geophys. Res. Lett.* 43, 7398–7407. doi:10.1002/2016gl069109
- Lauro, S. E., Pettinelli, E., Caprarello, G., Guallini, L., Rossi, A. P., Mattei, E., et al. (2021). Multiple Subglacial Water Bodies below the South Pole of Mars Unveiled by New MARSIS Data. *Nat. Astron.* 5, 63–70. doi:10.1038/s41550-020-1200-6
- Lin, S.-S., and Guro, M. D. (1998). Catalytic Decomposition of Hydrogen Peroxide on Iron Oxide: Kinetics, Mechanism, and Implications. *Environ. Sci. Technol.* 32, 1417–1423. doi:10.1021/es970648k
- Liochev, S. I., and Fridovich, I. (2002). The Haber-Weiss Cycle-70 Years Later: an Alternative View. *Redox Rep.* 7, 55–57. doi:10.1179/135100002125000190
- Liu, Z., Sleighter, R. L., Zhong, J., and Hatcher, P. G. (2011). The Chemical Changes of DOM from Black Waters to Coastal Marine Waters by HPLC Combined with Ultrahigh Resolution Mass Spectrometry. *Estuar. Coast. Shelf Sci.* 92, 205–216. doi:10.1016/j.ecss.2010.12.030
- Lovley, D. R., and Phillips, E. J. P. (1987). Rapid Assay for Microbially Reducible Ferric Iron in Aquatic Sediments. *Appl. Environ. Microbiol.* 53, 1536–1540. doi:10.1128/aem.53.7.1536-1540.1987
- Marsico, R. M., Schneider, R. J., Voelker, B. M., Zhang, T., Diaz, J. M., Hansel, C. M., et al. (2015). Spatial and Temporal Variability of Widespread Dark Production and Decay of Hydrogen Peroxide in Freshwater. *Aquat. Sci.* 77, 523–533. doi:10.1007/s00027-015-0399-2
- Mckay, G., Korak, J. A., Erickson, P. R., Latch, D. E., McNeill, K., and Rosario-Ortiz, F. L. (2018). The Case against Charge Transfer Interactions in Dissolved Organic Matter Photophysics. *Environ. Sci. Technol.* 52, 406–414. doi:10.1021/acs.est.7b03589
- Mcknight, D. M., Kimball, B. A., and Bencala, K. E. (1988). Iron Photoreduction and Oxidation in an Acidic Mountain Stream. *Science* 240, 637–640. doi:10.1126/science.240.4852.637
- Mcmahon, S., Bosak, T., Grotzinger, J. P., Milliken, R. E., Summons, R. E., Daye, M., et al. (2018). A Field Guide to Finding Fossils on Mars. *J. Geophys. Res. Planets* 123, 1012–1040. doi:10.1029/2017je005478
- Mesle, M. M., Beam, J. P., Jay, Z. J., Bodle, B., Bogenschütz, E., and Inskeep, W. P. (2017). Hydrogen Peroxide Cycling in High-Temperature Acidic Geothermal Springs and Potential Implications for Oxidative Stress Response. *Front. Mar. Sci.* 4. doi:10.3389/fmars.2017.00130
- Miller, G., and Zepp, R. G. (1979). Effects of Suspended Sediments on Photolysis Rates of Dissolved Pollutants. *Water Res.* 13, 453–459. doi:10.1016/0043-1354(79)90038-1
- Minor, E. C., Steinbring, C. J., Longnecker, K., and Kujawinski, E. B. (2012). Characterization of Dissolved Organic Matter in Lake Superior and its Watershed Using Ultrahigh Resolution Mass Spectrometry. *Org. Geochem.* 43, 1–11. doi:10.1016/j.orggeochem.2011.11.007
- Moffett, J. W., and Zajiriou, O. C. (1990). An Investigation Ofhydrogen Peroxide Chemistry in Surface Waters of Vineyard Sound with H218O2 and 18O2. *Limnol. Oceanogr.* 35, 1221–1229. doi:10.4319/lo.1990.35.6.1221
- Moffett, J. W., and Zika, R. G. (1987). Reaction Kinetics of Hydrogen Peroxide with Copper and Iron in Seawater. *Environ. Sci. Technol.* 21, 804–810. doi:10.1021/es00162a012
- Mopper, K., and Zhou, X. (1990). Hydroxyl Radical Photoproduction in the Sea and its Potential Impact on Marine Processes. *Science* 250, 661–664. doi:10.1126/science.250.4981.661
- Nye, J. J., Shock, E. L., and Hartnett, H. E. (2020). A Novel PARAFAC Model for Continental Hot Springs Reveals Unique Dissolved Organic Carbon Compositions. *Org. Geochem.* 141, 103964. doi:10.1016/j.orggeochem.2019.103964
- Orrego-Ruiz, J. A., Marquez, R. E., and Rojas-Ruiz, F. A. (2020). New Insights on Organic Geochemistry Characterization of the Putumayo Basin Using Negative Ion Electrospray Ionization Fourier Transform Ion Cyclotron Resonance Mass Spectrometry. *Energy fuels.* 34, 5281–5292. doi:10.1021/acs.energyfuels.9b02330
- Ossola, R., Tolu, J., Clerc, B., Erickson, P. R., Winkel, L. H. E., and McNeill, K. (2019). Photochemical Production of Sulfate and Methanesulfonic Acid from Dissolved Organic Sulfur. *Environ. Sci. Technol.* 53, 13191–13200. doi:10.1021/acs.est.9b04721
- Parenteau, M. N., and Cady, S. L. (2010). Microbial Biosignatures in Iron-Mineralized Phototrophic Mats at Chocolate Pots Hot Springs, Yellowstone National Park, United States. *Palaios* 25, 97–111. doi:10.2110/palo.2008.p08-133r
- Parenteau, M. N., Jahnke, L. L., Farmer, J. D., and Cady, S. L. (2014). Production and Early Preservation of Lipid Biomarkers in Iron Hot Springs. *Astrobiology* 14, 502–521. doi:10.1089/ast.2013.1122
- Paris, R., Desboeufs, K. V., and Journet, E. (2011). Variability of Dust Iron Solubility in Atmospheric Waters: Investigation of the Role of Oxalate Organic Complexation. *Atmos. Environ.* 45, 6510–6517. doi:10.1016/j.atmosenv.2011.08.068
- Parkhurst, D. L., and Appelo, C. (1999). User's Guide to PHREEQC (Version 2): A Computer Program for Speciation, Batch-Reaction, One-Dimensional Transport, and Inverse Geochemical Calculations. *Water-resources Investig. Rep.* 99, 312.
- Petasne, R. G., and Zika, R. G. (1997). Hydrogen Peroxide Lifetimes in South Florida Coastal and Offshore Waters. *Mar. Chem.* 56, 215–225. doi:10.1016/s0304-4203(96)00072-2
- Pierson, B. K., and Parenteau, M. N. (2000). Phototrophs in High Iron Microbial Mats: Microstructure of Mats in Iron-Depositing Hot Springs. *Fems Microbiol. Ecol.* 32, 181–196. doi:10.1111/j.1574-6941.2000.tb00711.x
- Poulin, B. A., Ryan, J. N., and Aiken, G. R. (2014). Effects of Iron on Optical Properties of Dissolved Organic Matter. *Environ. Sci. Technol.* 48, 10098–10106. doi:10.1021/es502670r
- Poulin, B. A., Ryan, J. N., Nagy, K. L., Stubbins, A., Dittmar, T., Orem, W., et al. (2017). Spatial Dependence of Reduced Sulfur in Everglades Dissolved Organic Matter Controlled by Sulfate Enrichment. *Environ. Sci. Technol.* 51, 3630–3639. doi:10.1021/acs.est.6b04142
- Powers, L. C., Babcock-Adams, L. C., Enright, J. K., and Miller, W. L. (2015). Probing the Photochemical Reactivity of Deep Ocean Refractory Carbon (DORC): Lessons from Hydrogen Peroxide and Superoxide Kinetics. *Mar. Chem.* doi:10.1016/j.marchem.2015.06.005

- Powers, L. C., Luek, J. L., Schmitt-Kopplin, P., Campbell, B. J., Magen, C., Cooper, L. W., et al. (2018). Seasonal Changes in Dissolved Organic Matter Composition in Delaware Bay, USA in March and August 2014. *Org. Geochem.* 122, 87–97. doi:10.1016/j.orggeochem.2018.05.005
- Powers, L. C., and Miller, W. L. (2016). Apparent Quantum Efficiency Spectra for Superoxide Photoproduction and its Formation of Hydrogen Peroxide in Natural Waters. *Front. Mar. Sci.* 3. doi:10.3389/fmars.2016.00235
- Ren, H., Sedlak, J. A., and Elrod, M. J. (2021). General Mechanism for Sulfate Radical Addition to Olefinic Volatile Organic Compounds in Secondary Organic Aerosol. *Environ. Sci. Technol.* 55, 1456–1465. doi:10.1021/acs.est.0c05256
- Riedel, T., Zark, M., Vahatalo, A. V., Niggemann, J., Spencer, R. G. M., Hernes, P. J., et al. (2016). Molecular Signatures of Biogeochemical Transformations in Dissolved Organic Matter from Ten World Rivers. *Front. Earth Sci.* 4. doi:10.3389/feart.2016.00085
- Ross, F., and Ross, A. B. (1977). *Selected Specific Rates of Reactions of Transients from Water in Aqueous Solution. III. Hydroxyl Radical and Peroxyhydroxyl Radical and Their Radical Ions*. USA: Notre Dame Univ. Radiation Lab.()
- Rossel, P. E., Stubbins, A., Hach, P. F., and Dittmar, T. (2015). Bioavailability and Molecular Composition of Dissolved Organic Matter from a Diffuse Hydrothermal System. *Mar. Chem.* 177, 257–266. doi:10.1016/j.marchem.2015.07.002
- Roth, V.-N., Lange, M., Simon, C., Hertkorn, N., Bucher, S., Goodall, T., et al. (2019). Persistence of Dissolved Organic Matter Explained by Molecular Changes during its Passage through Soil. *Nat. Geosci.* 12, 755–761. doi:10.1038/s41561-019-0417-4
- Ruff, S. W., and Farmer, J. D. (2016). Silica Deposits on Mars with Features Resembling Hot Spring Biosignatures at El Tatio in Chile. *Nat. Commun.* 7, 13554. doi:10.1038/ncomms13554
- Ruff, S. W., Farmer, J. D., Calvin, W. M., Herkenhoff, K. E., Johnson, J. R., Morris, R. V., et al. (2011). Characteristics, Distribution, Origin, and Significance of Opaline Silica Observed by the Spirit Rover in Gusev Crater, Mars. *J. Geophys. Res.-Planets* 116. doi:10.1029/2010je003767
- Rush, J. D., and Bielski, B. H. (1985). Pulse Radiolytic Studies of the Reactions of HO₂/O₂ with Fe (II)/Fe (III) Ions. The Reactivity of HO₂/O₂ with Ferric Ions and its Implication on the Occurrence of the Haber-Weiss Reaction. *J. Phys. Chem.* 89, 23. doi:10.1021/j100269a035
- Saladino, R., Botta, G., Delfino, M., and Di Mauro, E. (2013). Meteorites as Catalysts for Prebiotic Chemistry. *Chem. Eur. J.* 19 (50), 16916–16922. doi:10.1002/chem.201303690
- Schindelka, J., Iinuma, Y., Hoffmann, D., and Herrmann, H. (2013). Sulfate Radical-Initiated Formation of Isoprene-Derived Organosulfates in Atmospheric Aerosols. *Faraday Discuss.* 165, 237–259. doi:10.1039/c3fd00042g
- Schmitt-Kopplin, P., Gelencsér, A., Dabek-Zlotorzynska, E., Kiss, G., Hertkorn, N., Harir, M., et al. (2010). Analysis of the Unresolved Organic Fraction in Atmospheric Aerosols with Ultrahigh-Resolution Mass Spectrometry and Nuclear Magnetic Resonance Spectroscopy: Organosulfates as Photochemical Smog Constituents. *Anal. Chem.* 82, 8017–8026. doi:10.1021/ac101444r
- Scott, D. T., Runkel, R. L., Mcknight, D. M., Voelker, B. M., Kimball, B. A., and Carraway, E. R. (2003). Transport and Cycling of Iron and Hydrogen Peroxide in a Freshwater Stream: Influence of Organic Acids. *Water Resour. Res.* 39. doi:10.1029/2002wr001768
- Scully, N. M., McQueen, D. J., and Lean, D. R. S. (1996). Hydrogen Peroxide Formation: The Interaction of Ultraviolet Radiation and Dissolved Organic Carbon in Lake Waters along a 43–75°N Gradient. *Limnol. Oceanogr.* 41, 540–548. doi:10.4319/lo.1996.41.3.0540
- Shakeri Yekta, S., Gonsior, M., Schmitt-Kopplin, P., and Svensson, B. H. (2012). Characterization of Dissolved Organic Matter in Full Scale Continuous Stirred Tank Biogas Reactors Using Ultrahigh Resolution Mass Spectrometry: A Qualitative Overview. *Environ. Sci. Technol.* 46, 12711–12719. doi:10.1021/es3024447
- Sharpless, C. M., and Blough, N. V. (2014). The Importance of Charge-Transfer Interactions in Determining Chromophoric Dissolved Organic Matter (CDOM) Optical and Photochemical Properties. *Environ. Sci. Process. Impacts* 16, 654–671. doi:10.1039/c3em00573a
- Shean, D. (2006). Norris Geyser Basin's Dynamic Hydrothermal Features. *Yellowst. Sci.* 14, 24–28.
- Sleighter, R. L., Mckee, G. A., and Hatcher, P. G. (2009). Direct Fourier Transform Mass Spectral Analysis of Natural Waters with Low Dissolved Organic Matter. *Org. Geochem.* 40, 119–125. doi:10.1016/j.orggeochem.2008.09.012
- Sorey, M. L. (1991). *Effects of Potential Geothermal Development in the Corwin Springs Known Geothermal Resources Area, Montana, on the Thermal Features of Yellowstone National Park*. Reston, VA: US Geological Survey.
- Stenson, A. C., Marshall, A. G., and Cooper, W. T. (2003). Exact Masses and Chemical Formulas of Individual Suwannee River Fulvic Acids from Ultrahigh Resolution Electrospray Ionization Fourier Transform Ion Cyclotron Resonance Mass Spectra. *Anal. Chem.* 75, 1275–1284. doi:10.1021/ac026106p
- Tan, J., and Sephton, M. A. (2020). Organic Records of Early Life on Mars: The Role of Iron, Burial, and Kinetics on Preservation. *Astrobiology* 20, 53–72. doi:10.1089/ast.2019.2046
- Teixeira, H. D., Schumacher, R. I., and Meneghini, R. (1998). Lower Intracellular Hydrogen Peroxide Levels in Cells Overexpressing CuZn-Superoxide Dismutase. *Proc. Natl. Acad. Sci. U.S.A.* 95, 7872–7875. doi:10.1073/pnas.95.14.7872
- Tziotis, D., Hertkorn, N., and Schmitt-Kopplin, P. (2011). Kendrick-analogous Network Visualisation of Ion Cyclotron Resonance Fourier Transform Mass Spectra: Improved Options for the Assignment of Elemental Compositions and the Classification of Organic Molecular Complexity. *Eur. J. Mass Spectrom. (Chichester)* 17, 415–421. doi:10.1255/ejms.1135
- Vaghjiani, G. L., Turnipseed, A. A., Warren, R. F., and Ravishankara, A. R. (1992). Photodissociation of H₂O₂ at 193 and 222 Nm: Products and Quantum Yields. *J. Chem. Phys.* 96, 5878–5886. doi:10.1063/1.462684
- Van Kranendonk, M. J., Baumgartner, R., Djokic, T., Ota, T., Steller, L., Garbe, U., et al. (2021). Elements for the Origin of Life on Land: A Deep-Time Perspective from the Pilbara Craton of Western Australia. *Astrobiology* 21, 39–59. doi:10.1089/ast.2019.2107
- Voelker, B. M., Sedlak, D. L., and Zafiriou, O. C. (2000). Chemistry of Superoxide Radical in Seawater: Reactions with Organic Cu Complexes. *Environ. Sci. Technol.* 34, 1036–1042. doi:10.1021/es990545x
- Walling, C. (1975). Fenton's Reagent Revisited. *Acc. Chem. Res.* 8, 125–131. doi:10.1021/ar50088a003
- Wang, N., Zheng, T., Zhang, G., and Wang, P. (2016). A Review on Fenton-like Processes for Organic Wastewater Treatment. *J. Environ. Chem. Eng.* 4, 762–787. doi:10.1016/j.jece.2015.12.016
- Wang, Z., and Liu, J. (2014). New Insight into Photochemical Oxidation of Fe(II): The Roles of Fe(III) and Reactive Oxygen Species. *Catal. Today* 224, 244–250. doi:10.1016/j.cattod.2013.09.063
- Warren, L. A., and Ferris, F. G. (1998). Continuum between Sorption and Precipitation of Fe(III) on Microbial Surfaces. *Environ. Sci. Technol.* 32, 2331–2337. doi:10.1021/es9800481
- Weishaar, J. L., Aiken, G. R., Bergamaschi, B. A., Fram, M. S., Fujii, R., and Mopper, K. (2003). Evaluation of Specific Ultraviolet Absorbance as an Indicator of the Chemical Composition and Reactivity of Dissolved Organic Carbon. *Environ. Sci. Technol.* 37, 4702–4708. doi:10.1021/es030360x
- White, D. E., Hutchinson, R. A., and Keith, T. E. C. (1988). The Geology and Remarkable Thermal Activity of Norris Geyser Basin, Yellowstone National Park, Wyoming. *Prof. Pap.* 75, 1456.
- Wilson, C. L., Hinman, N. W., Cooper, W. J., and Brown, C. F. (2000a). Hydrogen Peroxide Cycling in Surface Geothermal Waters of Yellowstone National Park. *Environ. Sci. Technol.* 34, 2655–2662. doi:10.1021/es9906397
- Wilson, C. L., Hinman, N. W., and Sheridan, R. P. (2000b). Hydrogen Peroxide Formation and Decay in Iron-Rich Geothermal Waters: The Relative Roles of Abiotic and Biotic Mechanisms. *Photochem. Photobiol.* 71, 691–699. doi:10.1562/0031-8655(2000)071<0691:hpfadi>2.0.co;2
- Wong, G. T., Ku, T.-L., Liu, H., and Mulholland, M. (2015). *ts*, 117, 3–9. doi:10.1016/j.dsr2.2015.04.026 The Oceanography of the Northern South China Sea Shelf-Sea (NoSoCS) and its Adjacent Waters—Overview and Highligh *Deep Sea Res. Part II Top. Stud. Oceanogr.*
- Wuttig, K., Heller, M. L., and Croot, P. L. (2013). Pathways of Superoxide (O₂(-)) Decay in the Eastern Tropical North Atlantic. *Environ. Sci. Technol.* 47, 10249–10256. doi:10.1021/es401658t

- Yuan, X., Nico, P. S., Huang, X., Liu, T., Ulrich, C., Williams, K. H., et al. (2017). Production of Hydrogen Peroxide in Groundwater at Rifle, Colorado. *Environ. Sci. Technol.* 51, 7881–7891. doi:10.1021/acs.est.6b04803
- Zafriou, O. C., Voelker, B. M., and Sedlak, D. L. (1998). Chemistry of the Superoxide Radical (O₂⁻) in Seawater: Reactions with Inorganic Copper Complexes. *J. Phys. Chem. A* 102, 5693–5700. doi:10.1021/jp980709g
- Zepp, R. G., Sheldon, W. M., and Moran, M. A. (2004). Dissolved Organic Fluorophores in Southeastern US Coastal Waters: Correction Method for Eliminating Rayleigh and Raman Scattering Peaks in Excitation-Emission Matrices. *Mar. Chem.* 89, 15–36. doi:10.1016/j.marchem.2004.02.006
- Zhang, L.-S., and Wong, G. T. F. (1999). Optimal Conditions and Sample Storage for the Determination of H₂O₂ in Marine Waters by the Scopoletin-Horseradish Peroxidase Fluorometric Method. *Talanta* 48, 1031–1038. doi:10.1016/s0039-9140(98)00312-9
- Zhang, Y., and Blough, N. V. (2016). Photoproduction of One-Electron Reducing Intermediates by Chromophoric Dissolved Organic Matter (CDOM): Relation to O₂⁻ and H₂O₂ Photoproduction and CDOM Photooxidation. *Environ. Sci. Technol.* 50, 11008–11015. doi:10.1021/acs.est.6b02919
- Zhang, Y., Del Vecchio, R., and Blough, N. V. (2012). Investigating the Mechanism of Hydrogen Peroxide Photoproduction by Humic Substances. *Environ. Sci. Technol.* 46, 11836–11843. doi:10.1021/es3029582
- Zhao, Z., Gonsior, M., Schmitt-Kopplin, P., Zhan, Y., Zhang, R., Jiao, N., et al. (2019). Microbial Transformation of Virus-Induced Dissolved Organic Matter from Picocyanobacteria: Coupling of Bacterial Diversity and DOM Chemodiversity. *Isme J.* 13, 2551–2565. doi:10.1038/s41396-019-0449-1
- Zuo, Y., and Hoigne, J. (1992). Formation of Hydrogen Peroxide and Depletion of Oxalic Acid in Atmospheric Water by Photolysis of Iron(III)-oxalato Complexes. *Environ. Sci. Technol.* 26, 1014–1022. doi:10.1021/es00029a022

Conflict of Interest: The authors declare that the research was conducted in the absence of any commercial or financial relationships that could be construed as a potential conflict of interest.

Publisher's Note: All claims expressed in this article are solely those of the authors and do not necessarily represent those of their affiliated organizations, or those of the publisher, the editors and the reviewers. Any product that may be evaluated in this article, or claim that may be made by its manufacturer, is not guaranteed or endorsed by the publisher.

Copyright © 2022 Hinman, Mave, Powers, Schmitt-Kopplin, Cabrol and Gonsior. This is an open-access article distributed under the terms of the Creative Commons Attribution License (CC BY). The use, distribution or reproduction in other forums is permitted, provided the original author(s) and the copyright owner(s) are credited and that the original publication in this journal is cited, in accordance with accepted academic practice. No use, distribution or reproduction is permitted which does not comply with these terms.